Published in final edited form as:
Nature. 2016 July 14; 535(7611): 308–312. doi:10.1038/nature18610.

Ki-67 acts as a biological surfactant to disperse mitotic chromosomes

Sara Cuylen[1], **Claudia Blaukopf**[1], **Antonio Z. Politi**[2], **Thomas Müller-Reichert**[3], **Beate Neumann**[4], **Ina Poser**[5], **Jan Ellenberg**[2], **Anthony A. Hyman**[5], and **Daniel W. Gerlich**[1,*]

[1]Institute of Molecular Biotechnology of the Austrian Academy of Sciences (IMBA), Vienna Biocenter Campus (VBC), Dr. Bohr-Gasse 3, AT-1030 Vienna, Austria

[2]Cell Biology and Biophysics Unit, European Molecular Biology Laboratory (EMBL), Meyerhofstrasse 1, D-69117 Heidelberg, Germany

[3]Medical Faculty Carl Gustav Carus, Experimental Center, Technische Universität Dresden, Fetscherstrasse 74, D-01307 Dresden, Germany

[4]Advanced Light Microscopy Facility, European Molecular Biology Laboratory (EMBL), Meyerhofstrasse 1, D-69117 Heidelberg, Germany

[5]Max Planck Institute of Molecular Cell Biology and Genetics, Pfotenhauerstrasse 108, D-01307 Dresden, Germany

Summary

Eukaryotic genomes are partitioned into chromosomes, which during mitosis form compact and spatially well-separated mechanical bodies1–3.This enables chromosomes to move independently of each other for segregation of precisely one copy of the genome to each of the nascent daughter cells. Despite insights into the spatial organization of mitotic chromosomes4 and the discovery of proteins at the chromosome surface3,5,6, the molecular and biophysical basis of mitotic chromosome individuality have remained unclear. We report that Ki-67, a component of the mitotic chromosome periphery, prevents chromosomes from collapsing into a single chromatin mass after nuclear envelope disassembly, thus enabling independent chromosome motility and efficient interactions with the mitotic spindle. The chromosome separation function of Ki-67 is not confined within a specific protein domain but correlates with size and net charge of truncation mutants that apparently lack secondary structure. This suggests that Ki-67 forms a steric and electrical barrier, similar to surface-active agents (surfactants) that disperse particles or phase-

*Correspondence to: daniel.gerlich@imba.oeaw.ac.at.

Author contributions:
D.G. and S.C. conceived the project and designed experiments. B.N. and J.E generated siRNA library transfection plates. I.P. and A.A.H generated Ki-67-EGFP BAC cell pools. A.Z.P. and J.E. performed FCS measurements. D.G. and T.M.R. performed electron microscopy experiments. S.C. performed all other experiments and C.B. assisted in RNAi screen, chromosome spreads, cell line generation and cloning. D.G., S.C. and A.A.H. wrote the paper.

Author Information:
Reprints and permissions information is available at www.nature.com/reprints. The authors declare no competing financial interests. Readers are welcome to comment on the online version of the paper. Correspondence and requests for materials should be addressed to D.G. (daniel.gerlich@imba.oeaw.ac.at)

Europe PMC Funders Author Manuscripts

separated liquid droplets in solvents. Fluorescence correlation spectroscopy showed a high surface density of Ki-67 and dual-color labeling of both protein termini revealed an extended molecular conformation, indicating brush-like arrangements that are characteristic for polymeric surfactants. Our study thus elucidates a biomechanical role of the mitotic chromosome periphery and suggests that natural proteins can function as surfactants in intracellular compartmentalization.

Europe PMC Funders Author Manuscripts

To identify molecular factors that contribute to spatial separation of mitotic chromosomes we used an automated live-cell imaging pipeline. We visualized chromosome morphologies in HeLa cells stably expressing histone 2B (H2B) fused to a fluorescence resonance energy transfer (FRET) biosensor, which probes phosphorylation by the kinase Aurora B and thereby discriminates mitotic from interphase cells7. Addition of nocodazole excluded the effect of mitotic spindle perturbations. In this assay, we expected that depletion of any protein essential for chromosome separation would induce clusters of mitotic chromosomes, in contrast to the scattered chromosome distribution observed in control cells (Fig. 1a). We hence quantified the area of segmented chromosomes of live mitotic cells to detect clustering phenotypes (Fig. 1b).

Screening a small interfering RNA (siRNA) library targeting 1295 candidate genes, including a comprehensive list of factors required for mitosis8,9 and components of the chromosome periphery6 (Supplementary Table 1), revealed a single hit with three different siRNAs causing a chromosome clustering phenotype: Ki-67 (Fig. 1c and Extended Data Fig. 1a, b). We validated on-target specificity of the RNAi phenotype by Cas9 nickase-mediated synonymous mutations of the target region of one siRNA in all endogenous alleles of Ki-67 (Fig. 1d, e and Extended Data Fig. 1c-g).

Ki-67 is widely used as a proliferation marker in basic research and cancer prognosis10,11, yet its molecular mechanism is unknown. Clues might come from the localization of Ki-67 to the chromosome surface from prophase until telophase12,13, its requirement to target several other components of the mitotic chromosome periphery domain14,15, and its interaction with the kinesin Hklp216. While Ki-67 does not seem to contribute to the internal structure of mitotic chromosomes14, its depletion causes nucleolar reassembly defects during mitotic exit14 and misorganized interphase heterochromatin15. Given that we had screened for chromosome separation regulators, we re-examined a potential role of Ki-67 in mitotic chromosome individualization.

We imaged mitosis in HeLa, non-cancer hTERT-RPE1 cells, and mouse embryonic stem cells depleted of Ki-67. While metaphase plates in non-depleted control cells contained spatially separate chromosomes, they appeared as a single contiguous mass of chromatin in cells depleted of Ki-67 (Fig. 2a, Extended Data Fig. 2a-e). Time-lapse microscopy revealed that during prophase, when most chromosomes attach to the nuclear envelope17, chromosomes condensed into separate bodies in Ki-67-depleted cells, however soon after nuclear envelope breakdown (NEBD) chromosomes merged into a single coherent mass of chromatin (Fig 2b and Extended Data Fig. 2f, g). Furthermore, in wildtype cells Ki-67 relocalized from the nucleolus to chromosome arms only during very late prophase stages, after chromosome condensation had initiated (Extended Data Fig. 2h, i), and the internal structure of mitotic chromosomes appeared unaffected by Ki-67 depletion (Extended Data

Fig. 3)14. Hence, Ki-67 is not required for the initial chromosome individualization and condensation during prophase, but for the maintenance of spatial separation after nuclear envelope breakdown.

The unstructured morphology of metaphase plates in cells depleted of Ki-67 might result from increased adhesion between neighboring chromosomes. To test this, we tracked kinetochores in Ki-67-depleted cells stably expressing fluorescently labeled Centromere protein A (CENP-A) after mitotic entry in the presence of nocodazole (Fig. 2c, d). In control cells, chromosomes moved extensively by free diffusion. Mitotic chromosomes of Ki-67-depleted cells were, in contrast, almost as immobile as interphase chromosomes in control cells (Fig. 2e and Extended Data Fig. 4a-c, and Supplementary Video 1). Cell and nuclear size appeared normal and the nuclear envelope disassembled properly in Ki-67-depleted cells (Extended Data Fig. 4d-h and Supplementary Video 2). This suggests that mitotic chromosomes in Ki-67-depleted cells immobilize by increased adhesion rather than by spatial confinement.

A loss of spatial separation between mitotic chromosomes might impair spindle assembly and chromosome congression to the metaphase plate. Ki-67 depletion indeed substantially delayed progression from nuclear envelope disassembly until anaphase onset (Extended Data Fig. 5a). Under these conditions, however, chromosomes were still separated at the onset of spindle assembly through their preceding tether to the nuclear envelope (Fig. 2b, 0 min)17, which might enable microtubule access to kinetochores before chromosomes coalesce. To investigate more specifically how chromosome clustering affects chromosome congression, we depolymerized the spindle by nocodazole during mitotic entry and then imaged spindle assembly after nocodazole washout. Most control cells rapidly formed metaphase plates and entered anaphase, whereas Ki-67-depleted cells consistently failed to assemble metaphase plates and almost never entered anaphase (Fig. 2f, g). Imaging cells stably expressing the microtubule plus-tip marker EB3-EGFP showed rapid growth of microtubules into regions between neighboring chromosomes after nocodazole washout in control cells but much less in Ki-67-depleted cells (Extended Data Fig. 5b, c). Hence, Ki-67-dependent chromosome separation is important for efficient access of spindle microtubules and progression to anaphase.

To address the mechanism by which Ki-67 establishes a non-adhesive chromosome surface, we aimed to map this function to specific domains. To test the function of Ki-67 truncation mutants (Fig. 3a), we generated a Ki-67 knockout cell line, which clustered mitotic chromosomes similar to the Ki-67 RNAi phenotype (Fig. 3b, Extended Data Fig. 6a-g and Supplementary Video 3). That Ki-67 knockout cells survive despite the drastic chromosome coalescence phenotype might be explained by the initial separation of prophase chromosomes through tethers to the nuclear envelope17, which enables microtubule access to kinetochores prior to coalescence. However, the Ki-67 knockout cell line was sensitized to various stress conditions (Extended Data Fig. 6h), consistent with previous Ki-67 knockout studies15,18.

The N-terminus of Ki-67 contains a phosphopeptide-binding Forkhead-associated (FHA) domain19 and a Protein Phosphatase 1 (PP1)-binding site14. The central region consists of

16 tandem repeats20 and the C-terminal part is enriched in leucine and arginine (LR) residue pairs21. As expected, expression of full-length Ki-67 restored mitotic chromosome individualization in Ki-67 knockout cells (#1, Fig. 3b). Ki-67 lacking the C-terminal LR domain does not bind to chromosomes12 and it did not restore mitotic chromosome separation (#2, Fig. 3b) even if expressed at very high levels. A construct lacking the entire N-terminus, in contrast, restored mitotic chromosome separation, indicating that the binding sites for the known Ki-67 interactors Klp216, NIFK22, and PP114 are not relevant for this function (#4, Fig. 3b). A small Ki-67 fragment containing only half of the repeat domain and the chromosome-targeting LR domain still restored chromosome individualization, but the LR domain alone did not (#5 and #6, repectively, Fig. 3b). Unexpectedly, a complementary construct lacking the entire repeat domain also restored chromosome individualization (#7, Fig. 3b). Thus, any piece of the Ki-67 protein appears to support spatial separation as long as it is targeted to chromosomes by the LR-domain. To further test this, we designed a construct with randomly shuffled N-terminal fragments (#8, Fig. 3a). Remarkably, this construct also restored spatial separation of mitotic chromosomes in Ki-67 knockout cells (#8, Fig. 3b). Thus, Ki-67's chromosome-separating activity is not confined within a specific protein region.

We wondered whether general physico-chemical features of the Ki-67 protein might provide clues about its mechanism. Ki-67 is very large (325 and 360 kDa isoforms), has a very high net electrical charge (Extended Data Table 1), and is predicted to be mostly unfolded (Extended Data Fig. 7a). Furthermore, Ki-67 has an amphiphilic structure, as the short C-terminal LR domain of Ki-67 has high attraction to chromatin, while its long N-terminal domain has high attraction to the cytoplasm and is excluded from chromatin (Fig. 3b, # 6 and #2, respectively). An amphiphilic molecular structure combined with high electrical charge or long extensions (e. g. long hydrocarbon chains) are typical features of surface-active agents (surfactants), which are chemical reagents that disperse particles or phase-separated liquid droplets23.Through their localization at phase boundaries, surfactants stabilize dispersions and emulsions via steric hindrance and/or electrostatic repulsion23. The striking similarity of Ki-67 to surfactants prompted us to further explore this function.

If Ki-67 acted by steric or electrostatic repulsion similar to surfactants, reducing its size or charge by truncating the peptide chain should decrease the efficiency of knockout phenotype rescue.We indeed observed a more than 14-fold difference in the amount of protein required to restore spatial separation of mitotic chromosomes between the minimal truncation version bearing only half of the repeats and the LR domain, and full-length Ki-67 protein (Fig. 3c). The phenotype rescue efficiency correlated with the protein size and predicted net charge of the constructs (Fig. 3d), suggesting that the size and overall electric charge might be important for Ki-67's ability to space mitotic chromosomes apart.

If electrical charge were a key mechanism of mitotic chromosome separation, then other highly positively charged DNA-binding proteins might be able to substitute for Ki-67. Strikingly, individually overexpressed core histones separated mitotic chromosomes in Ki-67 knockout cells – yet only at very high overexpression levels and not as far apart as Ki-67 (Fig. 3e, and Extended Data Fig. 7b-h). This suggests that any positively charged chromosome-binding protein might separate mitotic chromosomes, yet Ki-67 apparently has

additional properties relevant for spacing chromosomes further apart, as for example its large size and its enrichment at the mitotic chromosome surface.

To form an effective repulsive barrier, Ki-67 should cover a substantial fraction of the mitotic chromosome surface. To investigate this, we tagged all endogenous alleles of Ki-67 with EGFP and measured the cytoplasmic concentration by fluorescence correlation spectroscopy (FCS) (Extended Data Fig. 8a-c). Using image segmentation of a reference DNA dye, we inferred that about 270,000 Ki-67 molecules bind to mitotic chromosomes, which corresponds to a surface density of about 210 Ki-67 molecules per square micrometer (Extended Data Fig. 8d-h) and an average spacing of 69 nm between Ki-67 molecules. Thus, Ki-67 is highly concentrated at the mitotic chromosome surface.

Polymeric surfactants adsorb at interfaces in a specific molecular orientation23 and they form extended brush-like structures at high concentrations24,25. Given the very C-terminal position of the chromatin-binding domain within Ki-67 and the exclusion of the remaining protein parts from chromatin regions (Fig. 3a, b), we probed the molecular extension of Ki-67 by attaching different fluorophores at each of its polypeptide ends (Extended Data Fig. 9a). Reference images of multispectral fluorescent beads showed that Gaussian fitting to fluorescence line profiles determines the relative localization of red and green fluorophores with an accuracy of 2.9 ± 2.2 nm (Extended Data Fig. 9b-d). We imaged live mitotic cells expressing mCherry-Ki-67-EGFP using confocal microscopy and determined the mean radial position of each fluorophore in perpendicularly sectioned chromosome arms (Fig. 4a, b). The N-terminal mCherry tag of Ki-67 localized 87.2 ± 45.7 nm outwards relative to the C-terminal EGFP tag, whereby a construct with inverted fluorophore positions and a control construct with both fluorophores attached to the N-terminus of Ki-67 yielded consistent results (Fig. 4c and Extended Data Fig. 9e-h). Thus, Ki-67 has a very elongated conformation that orients perpendicular to the surface of mitotic chromosomes, consistent with a brush-like arrangement.

High grafting densities of Ki-67 molecules at the chromosome surface might increase the height of brush-like structures, as described for non-biological surface-attached polymers24 (Extended Data Fig. 9i). Consistent with this, high overexpression levels of Ki-67 spaced mitotic chromosomes further apart than observed in wildtype cells (Fig. 4d, e). The range of Ki-67-mediated chromosome repulsion thus depends on molecular density.

Our study shows that Ki-67 is required to maintain individual mitotic chromosomes dispersed in the cytoplasm after their release from the mechanically rigid nuclear envelope. Ki-67 might provide this function through a surfactant mechanism at the phase boundary between mitotic chromatin and the cytoplasm (Fig. 4f).As phase separation has emerged as an important principle underlying the formation of many other membrane-less cell organelles like nucleoli or centrosomes25–27, it will be interesting to investigate whether and how natural protein surfactants might regulate other cellular phase boundaries.

Methods

Cell lines and cell culture

All cell lines used in this study have been regularly tested negatively for mycoplasm contamination. Their sources and authentication is summarized in Supplementary Table 2. HeLa cell lines stably expressing fluorescent reporter proteins were generated from a HeLa Kyoto cell line as previously described28. HeLa and hTERT-RPE1 cells were cultured in Dulbecco's modified Eagle medium (DMEM; Gibco) supplemented with 10% (v/v) fetal bovine serum (FBS; Gibco), 1% (v/v) penicillin-streptomycin (Sigma-Aldrich), 500 μg ml^{-1} G418 (Gibco) and 0,5 μg ml^{-1} puromycin (Calbiochem). CCE mouse embryonic stem cells were grown in gelatin-coated dishes in DMEM supplemented with 10% (v/v) FBS, 0.1 mM non-essential amino acids, 1 mM sodium pyruvate, 2 mM L-Glutamine, 0.05 mM β-mercaptoethanol, 1% penicillin-streptomycin, and 10^6 U/ml leukemia inhibitory factor. To visualize chromatin cell lines either stably expressed histone H2B fused to mCherry or mRFP (Fig. 2c-e, Extended Data Fig. 2h, i, 3 c-g, 4a-c, e, f, h), fused to the Aurora B FRET biosensor (Fig. 1b, c, 2b, f, g, Extended Data Fig. 2f, g, 5a) or were labeled with Hoechst/SiR-Hoechst as indicated. For mutation of the endogenous Ki-67 locus in HeLa wildtype cells CRISPR/Cas9 nickase strategy was applied as described in Extended Data Fig. 1c, d. SgRNAs were cloned into pSpCas9n(BB)-2A-GFP (pX461, Zhang lab29). A circular plasmid (pCR2.1, Life Technologies) carrying the mutation and 700 bp homology flanks on each site was used as a repair template for homologous recombination. The plasmid mix of guide RNA plasmids and the repair template was transfected into HeLa cells using X-tremeGENE 9 DNA transfection reagent (Roche). 2 days after transfection cells were sorted for the presence of Cas9 (GFP positive) and another 4 days later for the absence of Cas9 (GFP negative) using Fluorescence-activated cell sorting (FACS), either in batch or into 96 well plates, respectively. For endogenous EGFP tagging of Ki-67 in HeLa wildtype cells sgRNAs were cloned into pSpCas9n(BB) (pX335, Zhang lab29) and 1000 bp homology flanks were used. GFP positive cells were FACS sorted 6 days after transfection into 96 well plates. For live-cell imaging HeLa and RPE1 cell lines were grown either in 96-well plastic-bottom plates (μ clear; Greiner Bio-One), or on LabTek II chambered coverglass (Thermo Scientific). Live-cell imaging was performed in DMEM containing 10% (v/v) FBS and 1% (v/v) penicillin-streptomycin, but without phenol red and riboflavin to reduce autofluorescence28. CCE mouse embryonic stem cells were grown in LabTek II chambered coverglass (ThermoScientific) coated with 5 μg/ml Laminin-511 in PBS (BioLamina) for 2-3 h at 37°C. The fluorescence correlation spectroscopy measurements were performed in a CO_2 independent imaging medium (Gibco) supplemented with 20% FBS (v/v), 1 mM L-glutamine, 1 mM sodium pyruvate and 100 nM SiR-Hoechst.

Electron microscopy

For electron microscopy HeLa cells were grown on sapphire discs and cryo-immobilized using an EMPACT2+RTS high-pressure freezer (Leica Microsystems, Vienna, Austria). Specimens were frozen in 100 μm-deep membrane carriers (Leica) filled with growth medium containing 20% BSA (Sigma). Samples were freeze-substituted in acetone containing 1% osmium tetroxide and 0.1% uranyl acetate and thin-layer embedded in Epon-Araldite as described in 30. Serial thin sections were collected on Formvar-coated copper

slot grids and imaged in a TECNAI 12 electron microscope (FEI, The Netherlands) operated at 100 kV.

Western blotting

Cells were transfected with siRNAs in 6-well plates (Thermo Scientific) and 2-3 Mio. cells/ml were lysed in 1x SDS loading buffer at indicated time points after transfection. Protein samples were separated on NuPAGE Novex 3-8% Tris-Acetate protein gels (Life technologies) and transferred to a nitrocellulose membrane (Protran BA83, Sigma) by semidry blotting. Ki-67 was probed by monoclonal anti-Ki-67 SP6 antibody (abcam, ab16667) and actin by monoclonal anti-actin clone C4 (Milipore, MAB1501). Either fluorescently labeled antibodies (IRDye 800CW, IRDye 680RD; Odyssey) were used and membranes scanned on an Odyssey IR imager (LI-COR) or horseradish peroxidase-conjugated secondary antibodies (Biorad) were visualized using ECL Plus Western Blotting Substrate (Thermo Scientific) and films.

Plasmid and siRNA transfection

For transient or stable expression of fluorescently tagged marker proteins, the genes were subcloned into IRESpuro2 vectors that allow expression of resistance genes and tagged proteins from a single transcript (Supplementary Table 3). Plasmids were transfected into HeLa cells using X-tremeGENE9 DNA transfection reagent (Roche) or FuGene 6 transfection reagent (Promega) according to the manufacturer's instructions and imaged 48 h post transfection. siRNAs (Supplementary Table 4) were delivered with Lipofectamine RNAiMax (Invitrogen) at a final concentration of 10 nM according to the manufacturer's instructions. XWneg9 and Scrambled were used as non-targeting siRNA controls and 4 different siRNAs against Ki-67 were used (see below). Ki-67 #1 corresponds to Ki-5 published in Booth et al., 2014. Ki-67 siRNA #1 was used in Extended Data Fig.2b, c, e and 3c-h. Ki-67 siRNA #2 was used in Fig. 2b, Extended Data Fig. 2f, g, 3i and 4h, Ki-67 siRNA #4 was used in Fig. 2c-e and Extended Data Fig. 3a, b and 5b, c. All 4 Ki-67 siRNAs caused a similar chromosome coalescence phenotype as in Fig. 1d and 2a. A nuclear shape phenotype as described by Booth et al., 2014 (ref 14) was only observed with Ki-67 siRNA #1, but not with the other siRNAs that depleted Ki-67 protein with similar efficiency (see Extended Data Fig. 4d-g and 6f, g). All siRNAs were obtained from Life Technolgies as Silencer Select reagents. Imaging was performed 48 – 72 h post siRNA transfection as Western blotting (Extended Data Fig. 2b and 4d) indicated protein depletion to background levels.

Inhibitors and stains

Nocodazole (Sigma) was used at a final concentration of 100 ng ml^{-1} for 1 – 3 h to arrest cells in prometaphase. For washout experiments (Fig. 2f, g and Extended Data Fig. 5b, c) Labtek wells were washed 4x with 500 µl imaging medium without nocodazole before they were released into imaging medium. For acute addition during time-lapse imaging 400 ng ml^{-1} was used (Extended Data Fig. 3g). Hoechst 33342 (Sigma) was used at a final concentration of 0.2 µg ml^{-1}, SiR-Hoechst31 at concentrations of 100 – 200nM.

Europe PMC Funders Author Manuscripts

Ki-67 truncations

The long isoform of Ki-67 was cloned from HeLa cDNA into an IRESpuro2 vector under a CMV promoter and fused to mNeonGreen at the C-terminus. Truncation mutants were generated by PCR amplification, enzymatic digest and ligation from the full length construct (3256 amino acids) and cloned into the same plasmid. For truncation construct #2 amino acids 2929 - 3256 were removed, for construct #3 amino acids 1 - 134, for construct #4 amino acids 1 - 1002, for construct #5 amino acids 1 - 1970, for construct #6 amino acids 1 - 2930 and for construct #7 amino acids 995 - 2945. For construct #8, the N-terminal region from aa 1 - 994 was divided into 4 pieces and the order of the fragments was rearranged. The final construct contained the Ki-67 fragments in the following order: aa 507 - 726, aa 52 - 506, aa 727 - 994, aa 1 - 51 from N- to C-terminus.

RNAi screen

1295 genes were targeted by either two or three siRNAs. This target gene list included the MitoCheck genome-wide RNAi screen validation dataset with 1128 genes8, 100 predicted chromosome condensation factors 9 and 67 known and predicted chromosome periphery proteins (43 based on literature search, and additionally 24 based on Gene Ontology term and domain analysis in the dataset presented in 6). All siRNAs had been mapped against the 2013 human genome (ENSEMBL V70) to ensure unique target specificity. siRNAs were delivered using solid-phase reverse transfection32 in 384 well imaging plates (Falcon). Cells were seeded with 1 μM TO-PRO-3 Iodide (Life Technologies) on the screening plates using a Multidrop Reagent Dispenser (Thermo Scientific). 43 h after seeding nocodazole was added with the same device to a final concentration of 100 ng ml^{-1} and 6 hours later plates were imaged on a Molecular Devices ImageXpressMicro XL screening microscope (see below) using a x20, 0.75 NA S Fluor dry objective (Nikon) and acquiring 4 positions with 520 μm x 520 μm in each well. To compensate for inhomogeneous illumination, all images were flatfield corrected with the Metamorph software (Molecular Devices) using background images acquired in empty wells. Automated image analysis was performed using the in-house-developed CellCognition software33 and nuclei and sets of mitotic chromosomes were segmented by local adaptive thresholding. As a quality control for RNAi efficiency and specificity, supervised classification of cell morphologies was applied to the screening data and expected phenotypes8 were observed for all positive controls (siRNAs targeting INCENP, KIF11, PLK1, CDC20) and negative controls (empty, Scrambled or XWneg9 siRNA). For chromosome area measurements only live mitotic cells were taken into account using a 2 step gating strategy. First, mitotic cells were identified using the Aurora B FRET biosensor as depicted in Fig. 1b. Aurora B phosphorylation of the biosensor at the onset of mitosis causes a conformational change in the sensor that reduces FRET between a CFP for energy transfer (CyPet) donor and a YFP for energy transfer (YPet) acceptor7. To determine the range of FRET/YPet ratio of mitotic cells nocodazole arrested cells were identified by supervised classification using images from two untransfected wells of each plate. The 2.5th and 97.25th quantile of the background-subtracted FRET/YPet intensity of all prometaphase cells was used as lower and upper classification border, respectively ($0.6 < FRET/YPet > 0.82$). To identify dead cells and exclude them from further analysis, a TO-PRO-3 intensity threshold was applied ($TO\text{-}PRO\text{-}3 > 15$). From all live mitotic cells of each well the median size of the segmented chromosome area was calculated

and plotted either for each siRNA individually (Extended Data Fig. 1a) or as the mean of 2-3 siRNAs (Fig. 1c). Wells with > 20% apoptotic cells or < 20 live mitotic cells were excluded from the final analysis, as the chromosome area could not be reliably quantified under these conditions.

Live-cell microscopy

Automated wide-field fluorescence microscopy (Fig. 1) was performed on a Molecular Devices ImageXpressMicro XL screening microscope equipped with reflection-based laser autofocus and a x20, 0.75 NA S Fluor dry objective (Nikon), controlled by in-house-developed Metamorph macros33. Cells were maintained in a microscope stage incubator at 37°C in a humidified atmosphere of 5% CO_2. To image the Aurora B FRET cell line the following two filter sets were used: a FRET filter cube with an excitation filter 426 – 450 nm, emission filter 528.5 – 555.5 nm and a dichromatic mirror of 458 nm and a YFP filter cube with an excitation filter 488 - 512 nm, emission filter 528.5 – 555.5 nm, and a dichromatic mirror of 520 nm.

Confocal microscopy was performed on a customized Zeiss LSM780 microscope using a x40, 1.4 NA. Oil DIC Plan-Apochromat objective (Zeiss), controlled by ZEN 2011 software and an autofocus macro (AutofocusScreen, http://www.ellenberg.embl.de/index.php/software) provided by J. Ellenberg. The microscope was equipped with an incubation chamber (European Molecular Biology Laboratory (EMBL), Heidelberg, Germany), providing a humidified atmosphere at 37°C with 5% CO_2.

Fast time-lapse imaging with the EB3-GFP cell line was performed on a spinning-disk confocal microscope (UltraView VoX, PelkinElmer) with a x100, 1.45 NA objective controlled by Volocity software and equipped with an incubation chamber (EMBL) for imaging at 37°C with 5% CO_2.

For fluorescence recovery after photobleaching (FRAP) experiments, selected image regions were bleached using a laser intensity 600-fold higher than the laser intensity used for image acquisition, and the pixel dwell time was increased 20-fold above that used for image acquisition.

Immunostaining of mouse embryonic stem cells

Mouse embryonic stem cells were fixed in 3.7% formaldehyde in PBS for 10 min, washed twice with PBS containing 0.05% Tween20 and permeabilized with 0.5% Triton X-100 in PBS. Cells were blocked for 10 min with 10% FBS in PBS with 0.05% Tween20 and stained for 2 hours with a rabbit polyclonal anti-Ki-67 antibody (abcam, ab66155, 1:300). After several washes cells were stained with anti-rabbit IgG Alexa Fluor 488 (Molecular Probes, 1:600). DNA was stained with 0.8 μg ml^{-1} Hoechst 33342 (Sigma).

Mitotic chromosome spreads

HeLa cells treated with siRNA for 48 h were trypsinized and resuspended in 75 mM KCl for 16 min at 37°C. Cells were then fixed by 3:1 ice-cold methanol:acetic acid for 15 min at 4°C. After 2 washes with 3:1 ice-cold methanol:acetic acid cells were dropped on cleaned

and pre-chilled glass slides from a height of 30 cm. Cells were dried on the slide and mounted in Vectashield mounting medium with 1.5 μg/ml DAPI (Vector Laboratories).

Micrococcal nuclease hypersensitivity assay

HeLa cells treated with siRNA for 48 h were trypsinized and washed twice with PBS. 10 Million cells per sample were resuspended in lysis buffer (25 mM Tris pH 7.5, 100 mM NaCl, 5 mM $MgCl_2$, 0.2% NP-40, 1x Complete EDTA-free protease inhibitor (Roche)) and lysed on ice by passing 20 times through a needle (0.4 mm). Chromatin fraction was pelleted by centrifugation, washed once with micrococcal nuclease (MNase) digestion buffer (10 mM Tris pH 7.4, 15 mM NaCl, 60 mM KCl, 1 mM $CaCl_2$), resuspended in MNase digestion buffer and aliquoted. Aliquots were prewarmed to 37°C for 2 min and subsequently incubated with threefold serial dilutions of micrococcal nuclease from 0.06 U/ml to 45 U/ml (Thermo Scientific) for 20 min at 37°C in MNase digestion buffer. The reaction was stopped by addition of 25 mM EDTA. 1% SDS was added, the sample was diluted 1:4 with deionized water and 500 mM NaCl was added. DNA was phenol-chloroform extracted and run on a 1.5% agarose gel.

Colony formation assay

200 HeLa wildtype or Ki-67 knockout cells were seeded into 6-well plates. After two days indicated drugs were added at increasing concentrations and plates were incubated for 10 – 17 days. Colonies were then fixed with 4% formaldehyde for 20 minutes, washed with water, stained for 20 – 30 min with Crystal Violet, washed with water several times and dried.

Secondary structure and charge predictions

Folded and charged regions within Ki-67 were visualized with FoldIndex (http://bip.weizmann.ac.il/fldbin/findex) and the EMBOSS charge prediction tool (http://www.bioinformatics.nl/cgi-bin/emboss/charge). A proteome-wide net charge analysis was performed on the human proteome assembly GRCh38 using a customized R script based on the net charge calculation function of the ‘seqinr’ R package and pK values from EMBOSS (Extended Data Table 1).

Statistical analysis and sample numbers

All experiments were repeated several times and indicated experiment numbers always refer to biological replicates. Data were tested for normality and equal variances with Shapiro-Wilk and Levene’s tests ($\alpha = 0.05$), respectively. The appropriate statistical test was chosen as follows: Unpaired normal distributed data were tested with a two-tailed t-test (in case of similar variances) or with a two-tailed t-test with Welch’s correction (in case of different variances). Unpaired not normal distributed data were tested with two-tailed Mann-Whitney test (in case of similar variances) or with a two-tailed Kolmogorov-Smirnov test (in case of different variances). Paired not normal distributed data were tested with a Wilcoxon matched-pairs signed rank test.

Sample numbers of Fig. 1e: 3 experiments with the following sample numbers in wildtype cells: No siRNA (n = 435, 242, 327), siControl (n = 856, 472, 506), siKi-67 #1 (n = 422,

241, 201), siKi-67 #2 (n = 480, 318, 331), siKi-67 #3 (n = 961, 444, 466), siKi-67 #4 (n = 859, 560, 492). 3 experiments with the following sample numbers in siKi-67 #2 resistant cells: No siRNA (n = 331, 325, 235), siControl (n = 932, 291, 367), siKi-67 #1 (n = 427, 227, 71), siKi-67 #2 (n = 498, 223, 185), siKi-67 #3 (n = 331, 385, 298), siKi-67 #4 (n = 847, 223, 245).

Extended Data

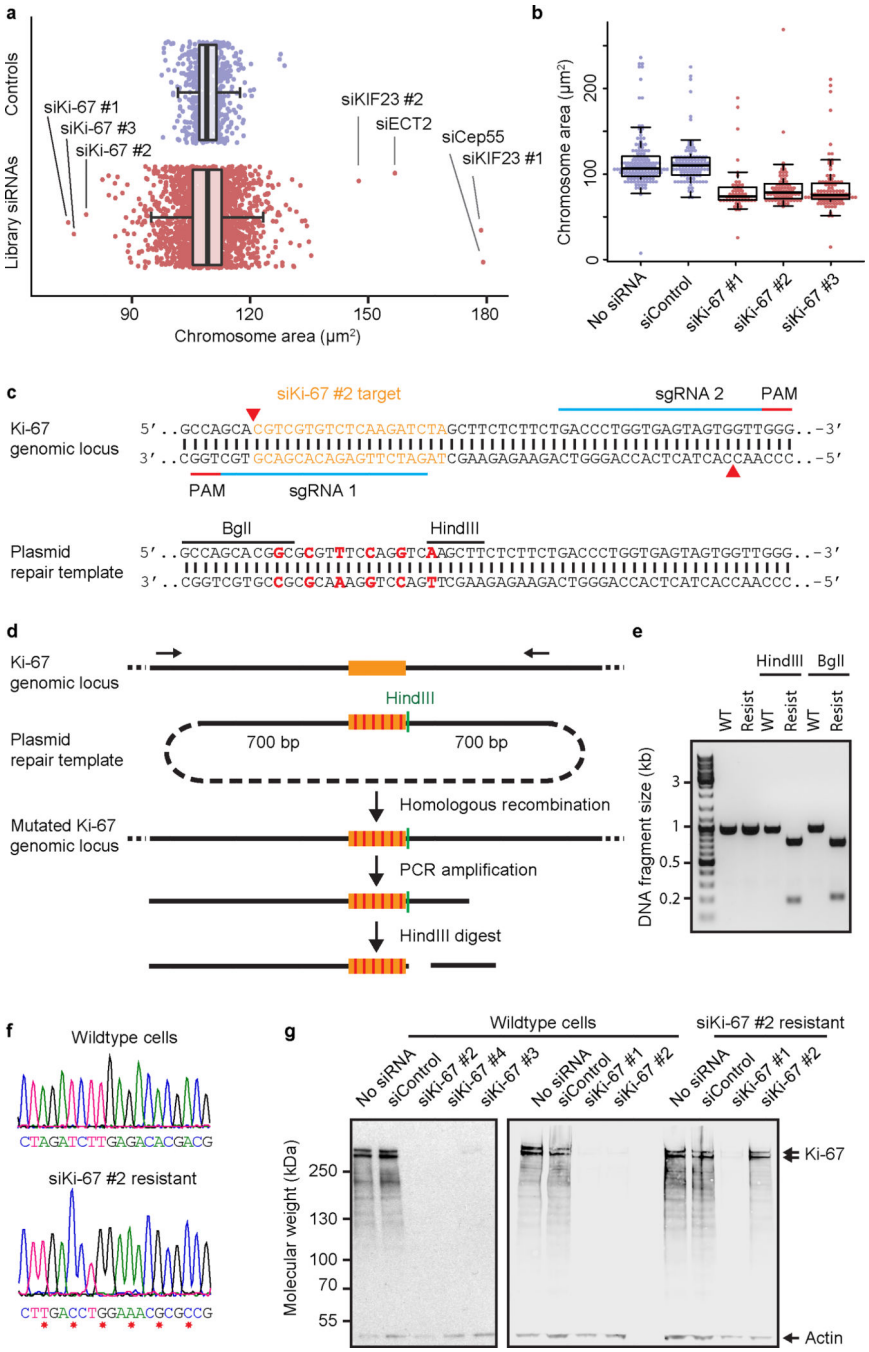

Europe PMC Funders Author Manuscripts

Europe PMC Funders Author Manuscripts

Extended Data Figure 1. Generation of a Ki-67 siRNA #2-resistant HeLa cell line by homozygous mutation of endogenous Ki-67 genomic loci.

a, Quantification of chromosome area as in Fig. 1b, but displayed for each individual siRNA, shows that the three siRNAs causing strongest chromosome clustering all target Ki-67. Each data point corresponds to the median chromosome area of all live mitotic cells in a specific siRNA condition. Median, quartiles and 1.5 * interquartile range of controls (siControls and untransfected) and the siRNA library are indicated. The top four siRNAs causing an increased chromosome area all target proteins involved in cytokinesis. Hence the chromosome area increase is likely to be a consequence of polyploidization by cytokinesis failure in preceding divisions. **b**, Chromosome areas of all individual live mitotic cells from the original RNAi screening data. Each data point corresponds to the chromosome area in a single cell. This reveals that the clustering phenotype is very penetrant within the cell population. **c**, CRISPR/Cas9 nickase strategy to mutate the siKi-67 #2 target site without changing the amino acid coding sequence. Red triangles indicate DNA strand nicking sites. PAM: Protospacer Adjacent Motif. sgRNA: single guide RNA. **d**, Schematic of genotyping strategy. A newly generated HindIII (or BglI) restriction site generated by CRISPR/Cas9 nickase as depicted in c was used to detect correctly mutated alleles. **e**, HindIII and BglI restriction fragments were detected by gel electrophoresis following the assay depicted in d, showing successful recombination of all three Ki-67 alleles present in HeLa cells. **f**, DNA sequencing chromatogram of the siKi-67 #2 target site of a wildtype and the CRISPR/Cas9-mutated cell line, respectively. Asterisks indicate mutated nucleotides. **g**, Western blot performed on whole cell lysates of wildtype or siKi-67 #2 resistant cell lines 48 h after indicated siRNA transfections demonstrates that all siRNAs used in this study (siKi-67 #1-4) efficiently depleted Ki-67 in wildtype cells and that the CRISPR/Cas9 mutated cell line was fully resistant against siKi-67 #2 but still sensitive to siKi-67 #1. The two bands labeled by anti Ki-67 antibody correspond to the two Ki-67 isoforms with predicted molecular masses of 320 and 359 kDa.

Europe PMC Funders Author Manuscripts

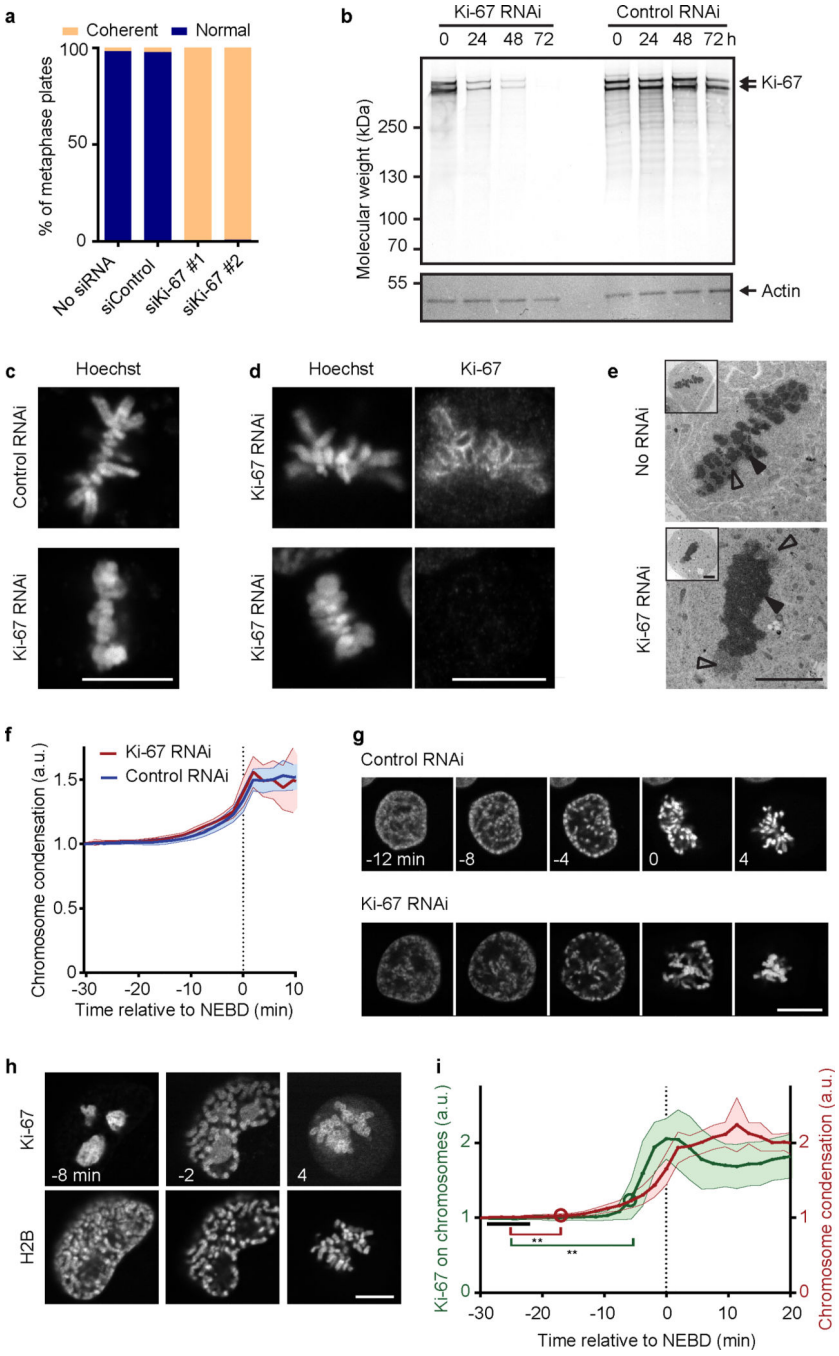

Extended Data Figure 2. Ki-67 is not required for initial chromosome individualization and condensation but for maintenance of chromosome separation.

a, Quantification of phenotype penetrance in Fig. 2a. Live metaphase cells recorded by an automated imaging pipeline were classified as coherent or normal by supervised machine learning (3 independent experiments with total sample numbers of n = 111 (no siRNA), n = 88 (siControl), n = 112 (siKi-67 #1), n = 131 (siKi-67 #2)). **b**, Western blot analysis of HeLa wildtype cells, performed at indicated time points after siKi-67 #1 transfection, showed efficient depletion of Ki-67 at 48 – 72 h post siRNA transfection. This time window was

Europe PMC Funders Author Manuscripts

hence used for all further experiments. For gel source data, see Supplementary Fig. 1. **c**, Live hTERT-RPE1 cells stained with Hoechst were imaged 48 h after siRNA transfection. Control cells (n = 21) had spatially separate chromosomes, whereas Ki-67 siRNA-transfected cells (n = 17) had metaphase plates that appeared as a contiguous mass of chromatin. **d**, Mouse embryonic stem cells were fixed 48 h after siRNA transfection and stained using anti-Ki-67 antibody and Hoechst. Metaphase plates that lacked Ki-67 signal had chromosomes merged into an unstructured mass of chromatin (lower panel), whereas all cells with residual levels of Ki-67, owing to incomplete RNAi-mediated protein depletion, had normal metaphase plate morphologies. Representative examples for n = 20 cells. **e**, Electron micrographs of HeLa cells transfected with siRNAs as indicated demonstrate that chromosomes appeared as a single contiguous mass. Representative images for n = 10/10 control and 9/11 for Ki-67 RNAi cells. Closed arrowheads mark dark chromatin areas; open arrowheads mark lighter grainy layer of chromosome periphery. **f**, Quantification of prophase chromosome condensation using pixel intensity standard deviation of the H2B-mCherry fluorescence as a measure for homogeneity of chromatin. Curves indicate mean and SD of 16 cells per condition. **g**, Representative example cells of the chromosome condensation assay in f. **h**, Ki-67 localization on chromosomes in live prophase HeLa cells expressing H2B-mCherry/Ki-67-EGFP (NEBD, t = 0 min) **i**, was quantified (excluding nucleoli) during mitotic entry. A significant change ($p < 0.01$ by Student's t-test) in chromosome condensation (marked by red circle; compared to the initial 4 frames) occurs 11 min before a significant increase in Ki-67 localization (green circle). Curves indicate mean and SD of 13 cells. Bars, 5 μm in e, all others 10 μm.

Europe PMC Funders Author Manuscripts

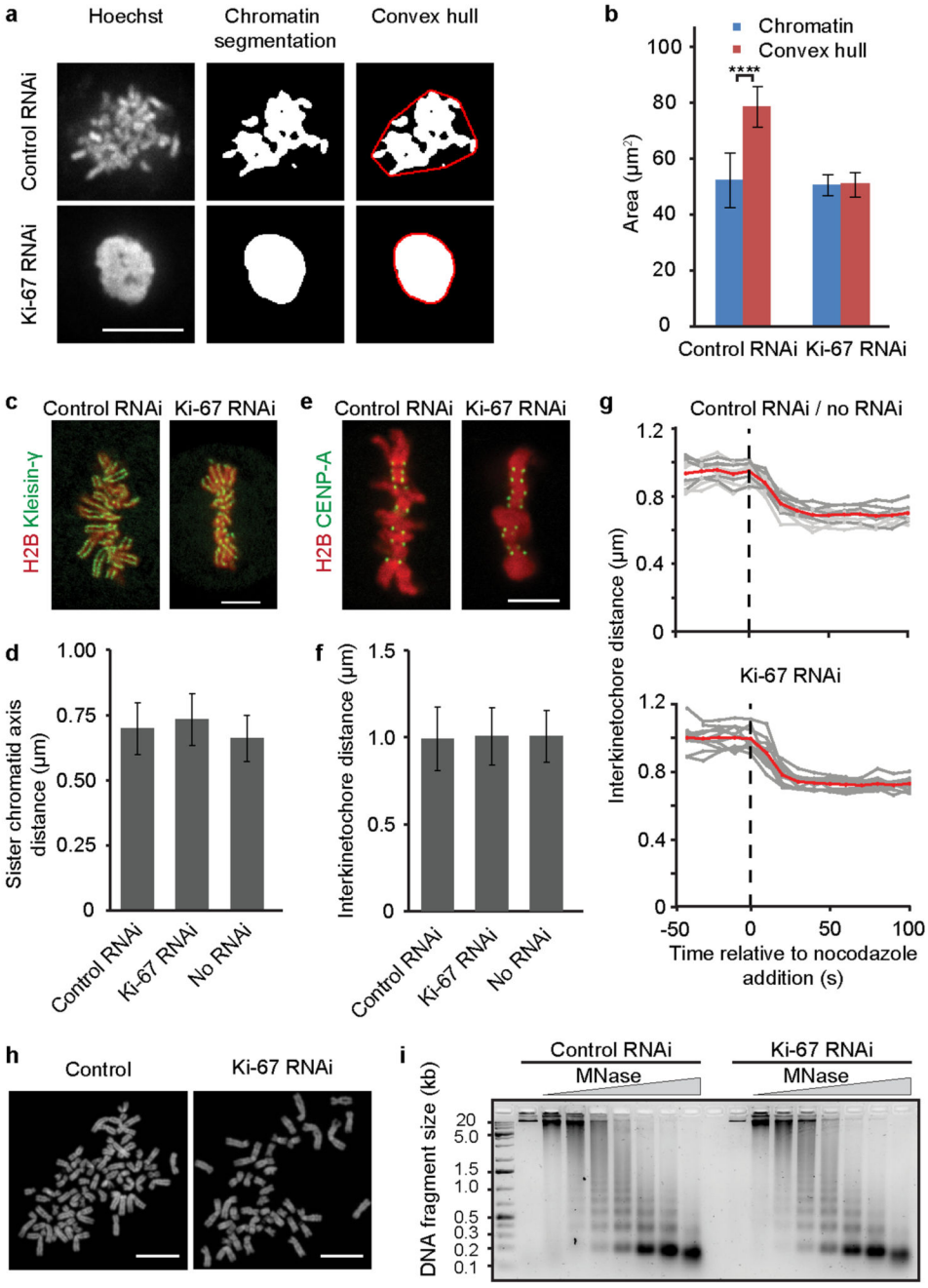

Extended Data Figure 3. Internal chromosome organization is not affected by Ki-67 depletion.

a, Hoechst-stained chromosomes of control or Ki-67-depleted HeLa cells were segmented by thresholding, subsequently a convex hull was fitted around segmented chromosomes (red line) and **b**, the segmented chromatin area and area of a convex hull fit were quantified. The calculated chromatin area of Ki-67 depleted cells was similar to control depleted cells, which demonstrates that Ki-67 depletion has no detectable effect on chromosome-internal compaction. Ki-67 depleted cells lack inter-chromosomal space as the convex hull area is almost identical with the chromatin area (n = 16 for each siRNA, bars indicate mean ± SD,

**** indicates $p < 0.0001$ by paired Wilcoxon matched-pairs signed rank test). **c**, Live HeLa cell expressing H2B-mCherry/EGFP-Kleisin-γ were imaged 72 h after siKi-67 #1 or control siRNA transfection and **d**, mean and SD of sister chromosome axis distance were quantified (n = 508 from 3 experiments (control RNAi), n = 380 from 4 experiments (Ki-67 RNAi), n = 398 from 3 experiments (no RNAi)). **e**, Live HeLa cell stably expressing H2B-mCherry/CENP-A-EGFP were imaged ~60 h after siKi-67 #1 or control siRNA transfection and **f**, mean and SD of interkinetochore distance were quantified (n = 875 from 3 experiments (control RNAi), n = 1489 from 5 experiments(Ki-67 RNAi), n = 818 from 3 experiments (no RNAi)). **g**, Centromere elasticity assay. Metaphase HeLa cells stably expressing H2B-mCherry/CENP-A-EGFP were imaged with 10 s time-lapse before and after nocodazole addition. The interkinetochore distance measurement over time in 12 control cells (control siRNA = light gray and untransfected cells = dark gray) and 10 cells transfected with siKi-67 #1 (gray lines) demonstrated that kinetochores were under tension in Ki-67 depleted cells. The red line indicates the mean. **h**, Chromosome spreads of untransfected or Ki-67 depleted HeLa cells appeared similar. Representative examples of 35 chromosome spreads from 2 independent experiments are depicted. **i**, Nuclei from control or Ki-67 depleted HeLa cells were treated with titrated amounts of MNase and DNA was subjected to 1.5% agarose electrophoresis. No detectable difference was seen in two independent experiments. Bars, 10 μm in a, h, 5 μm in c, e.

Europe PMC Funders Author Manuscripts

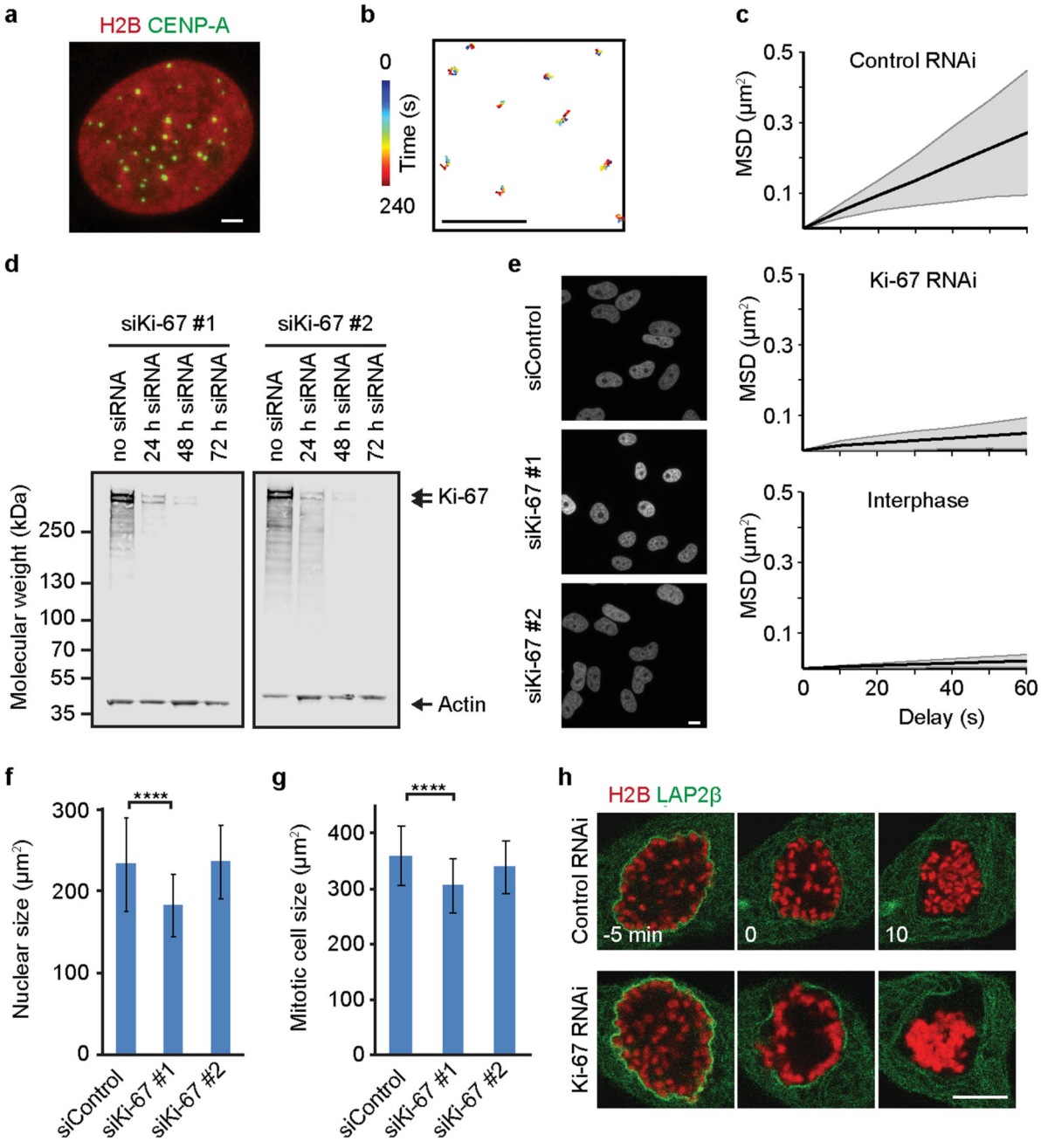

Extended Data Figure 4. Chromosome clustering and motility decrease are not caused by spatial confinement.

a-b, Representative example of kinetochore tracking performed in interphase (quantified in Fig. 2e). **a**, Live interphase HeLa cells stably expressing H2B-mCherry/CENP-A-EGFP were imaged in presence of nocodazole and **b**, kinetochores were tracked in time-lapse videos. **c**, Representative MSD analyses of kinetochore tracks (CENP-A-EGFP) of mitotic HeLa cells (from Fig. 2c, d) and of the interphase cell in panel a. **d**, Western blot analysis of HeLa wildtype cells, performed at indicated time points after siKi-67 #1 or #2 transfection

confirmed that both siRNAs deplete Ki-67 protein with similar efficiency. **e**, Interphase cells expressing H2B-mCherry 48 h after indicated siRNA transfections **f**, were quantified with regard to nuclear size by automated segmentation of H2B-mCherry (bars indicate mean ± SD, **** indicates $p < 0.0001$ by Kolmogorov-Smirnov test, data from 25 random positions: n = 303 (siControl), n = 303 (siKi-67 #1), n = 246 (siKi-67 #2)). Only siKi-67 #1 caused a significant decrease in nuclear size while siKi-67 #2, which was used for kinetochore tracking in Fig. 2c-e, had no effect on nuclear size. As Ki-67 knockout cells also had a normal nuclear size (Extended Data Figure 6f, g), we conclude that the effect of siKi-67 #1 on nuclear size is likely due to off-target protein depletion. **g**, Quantification of mitotic cell size of control or Ki-67 depleted cells demonstrated that similar to f, only siKi-67 #1 led to a significant decrease in cell size consistent with an off-target effect (bars indicate mean ± SD, **** indicates $p < 0.0001$ by Mann-Whitney test, total sample numbers: n = 74 (siControl), n = 100 (siKi-67 #1), n = 95 (siKi-67 #2)). As kinetochore tracking was based on siKi-67 #2, the reduced motility of mitotic chromosomes cannot be attributed to cell size changes. **h**, Live HeLa cells stably expressing H2B-mRFP/LAP2β-EGFP were imaged 48 h after siRNA transfection as they entered mitosis in the presence of nocodazole (n = 15 per condition). Bars, 2 μm in a, b, 10 μm in e, h.

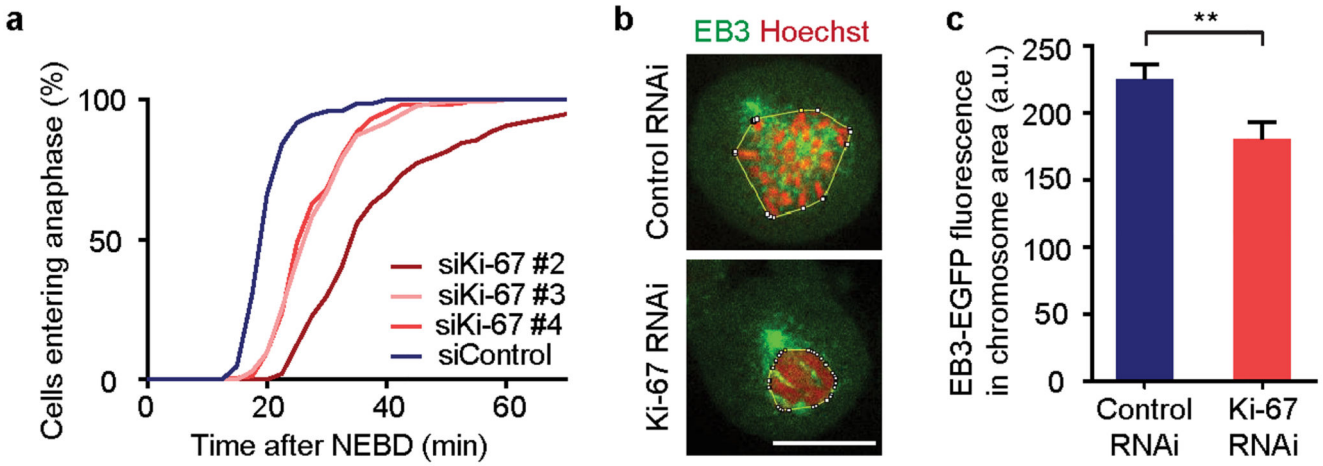

Extended Data Figure 5. Ki-67 depletion causes a prolonged mitosis and impairs access of spindle microtubules to chromosomes.

a, Mitotic progression determined by live-cell microscopy of HeLa cells expressing H2B-Aurora B FRET biosensor, after siRNA transfection as indicated. 3 independent experiments with total sample numbers of n = 145 (siControl), n = 97(siKi-67 #2), n = 134 (siKi-67 #3),n = 164 (siKi-67 #4). **b**, Live HeLa cells stably expressing EB3-EGFP were imaged 2 minutes after release from a 2 h nocodazole treatment, chromosome areas were identified (yellow lines) and **c**, EB3-EGFP mean fluorescence was measured in chromosome areas (bars indicate mean and SEM from 50 cells per condition, ** indicates $p < 0.01$ by Mann-Whitney test). Bar, 10 μm.

Europe PMC Funders Author Manuscripts

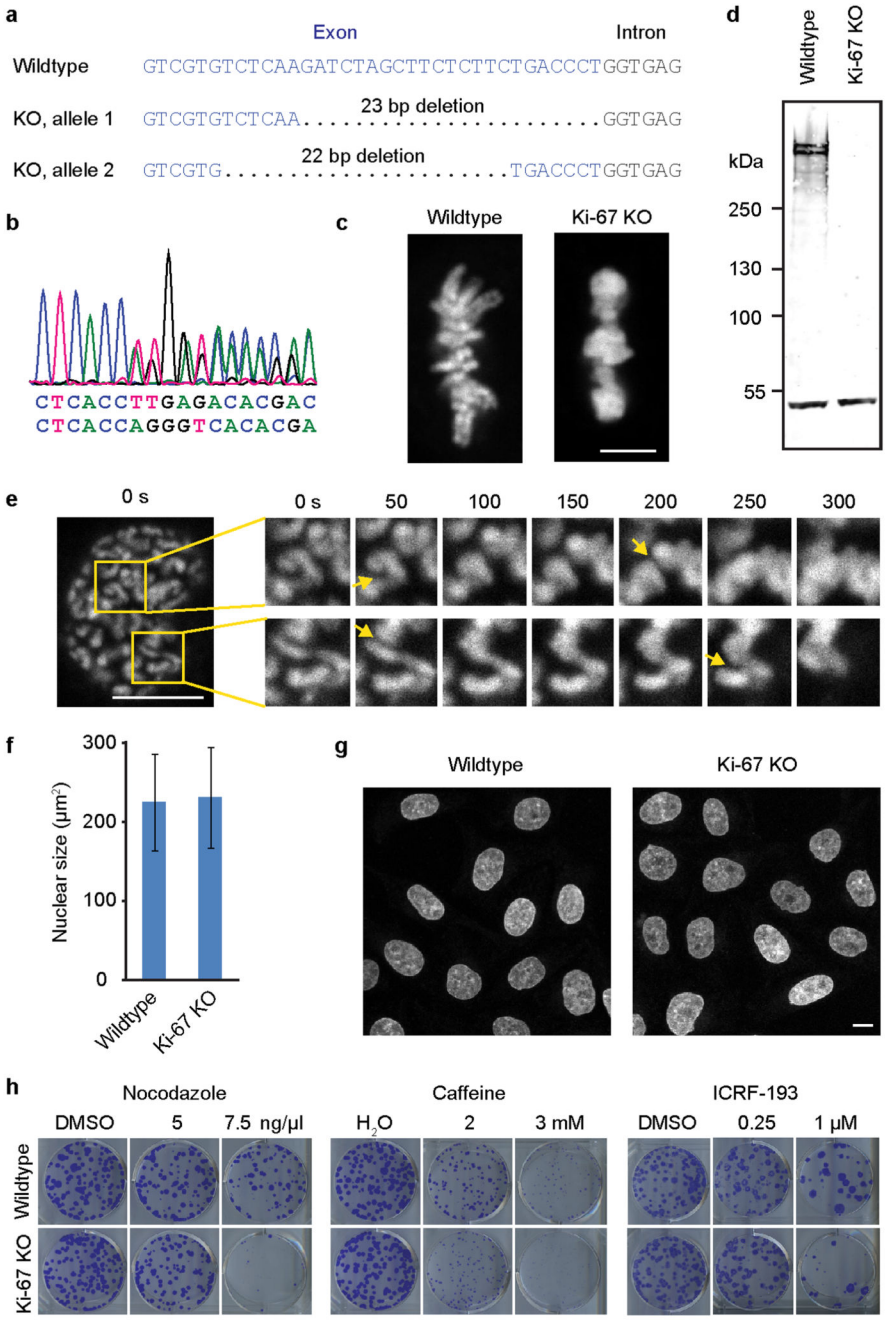

Extended Data Figure 6. Generation of a Ki-67 knockout cell line.

a, CRISPR/Cas9 was used to generate a HeLa cell line with indicated deletions on exon 5 of the Ki-67 allele. **b**, DNA sequencing chromatogram confirmed that no further alleles are present. **c**, Metaphase plates of live HeLa wildtype and Ki-67 knockout cells stained with Hoechst (n = 30 per cell line). **d**, Western blot performed on whole cell lysates of wildtype or Ki-67 knockout cells. The two high molecular weight bands labeled by anti Ki-67 antibody in wildtype that correspond to the two Ki-67 isoforms are undetectable for Ki-67 knockout cells. Actin was used as a loading control. **e**, Representative time-lapse image

Europe PMC Funders Author Manuscripts

series of a Ki-67 knockout cell proceeding from prophase to prometaphase in the presence of nocodazole (n = 12, see Supplementary Video 3). Chromosomes are labeled with SiR-Hoechst and two regions were selected to exemplify coalescence of chromosomes upon their close approach. Arrows mark regions just before their coalescence. **f**, Automated segmentation of SiR-Hoechst-labeled interphase nuclei of wildtype and Ki-67 knockout cells confirmed a normal nuclear size of Ki-67 knockout cells (mean and SD of 200 wildtype and 270 Ki-67 KO cells). **g**, Representative example images of interphase wildtype or Ki-67 knockout cells stained with SiR-Hoechst of the quantification in f. **h**, The sensitivity of Ki-67 knockout cells to low dose nocodazole, caffeine or a topoisomerase II inhibitor (ICRF-193) was compared to wildtype by a colony formation assay. Representative images from two to three independent experiments are shown. Bar, 5 μm in c, 10 μm in e, g.

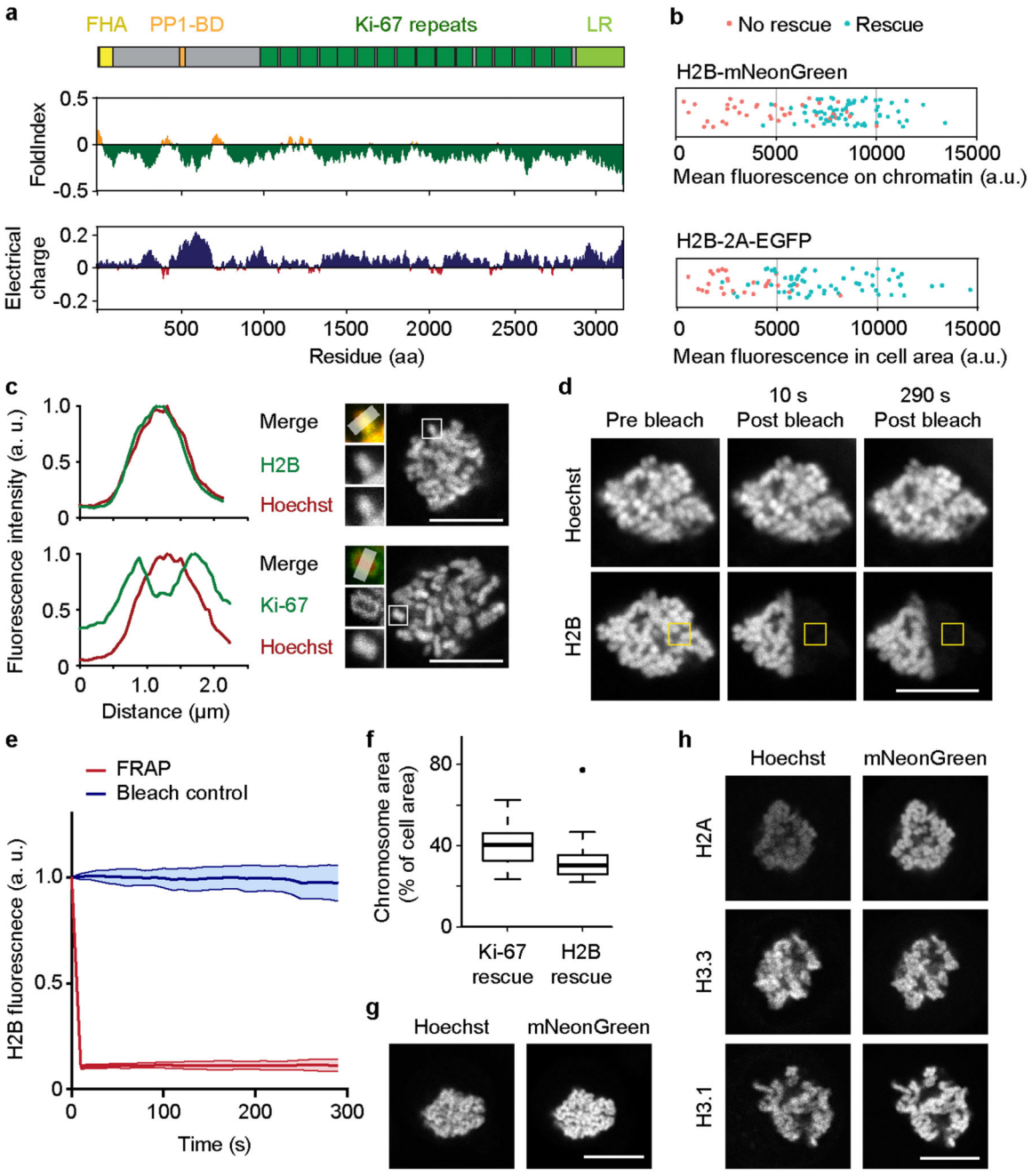

Extended Data Figure 7. Ki-67 has little secondary structure, is highly positively charged, and its absence can be partly compensated by overexpression of core histones.

a, Folding and charge prediction of full length Ki-67 based on FoldIndex and EMBOSS webtools using a sliding window of 100. Unfolded regions are depicted in green, folded regions in orange. Positive charge is marked in blue, negative charge in red. **b**, Quantification of overexpressed histone levels in individual cells related to the mitotic chromosome morphology phenotype, classified by visual inspection. Note that the mean fluorescence values are not comparable to Fig. 3c as different imaging settings had to be

Europe PMC Funders Author Manuscripts

used. Cells are from 4-5 independent experiments. **c**, Radial localization of overexpressed H2B-mNeonGreen in live Ki-67 knockout cells (n = 20). Normalized fluorescence intensity along line profiles across a chromosome arm of live Ki-67 knockout cells transiently transfected with H2B-mNeonGreen (upper panel) or Ki-67-mNeonGreen (lower panel) indicate that overexpressed H2B binds to the surface as well as internal region within chromosomes. **d**, **e**, Stable association of H2B-mNeonGreen with mitotic chromosomes. **d**, Half of the mitotic chromosomes in Ki-67 knockout cells highly overexpressing H2B-mNeonGreen were photobleached and the recovery of fluorescence was followed by time-lapse recording in an image region (yellow box). Representative example of the quantification in e. **e**, Curves indicate mean and SD of 20 photobleached and 19 unbleached control cells. **f**, Quantification of mitotic chromosome area relative to total cell area for cells shown in panel b and Fig. 3c. Boxes indicate median, quartiles and 1.5 * interquartile range (n = 30 for Ki-67, n = 64 for H2B). **g**, Live Ki-67 knockout cell transiently transfected with a H2B-mNeonGreen and stained with SiR-Hoechst. While 25 of 64 rescued cells displayed fully separated chromosomes (Fig. 3e), a large fraction of cells (39 of 64 rescued cells) showed detectable chromosome individualization at a lower extent compared to wildtype cells. Representative single z-section of the latter is shown. **h**, Live Ki-67 knockout cells transiently transfected with plasmids for expression of the indicated histone fused to mNeonGreen and stained with SiR-Hoechst. Representative single z-sections of 12-18 cells from 2-3 independent experiments are depicted. Although chromosome individualization was restored, chromosomes were not separated to the same extent as in wildtype cells. Bars, 10 μm.

Europe PMC Funders Author Manuscripts

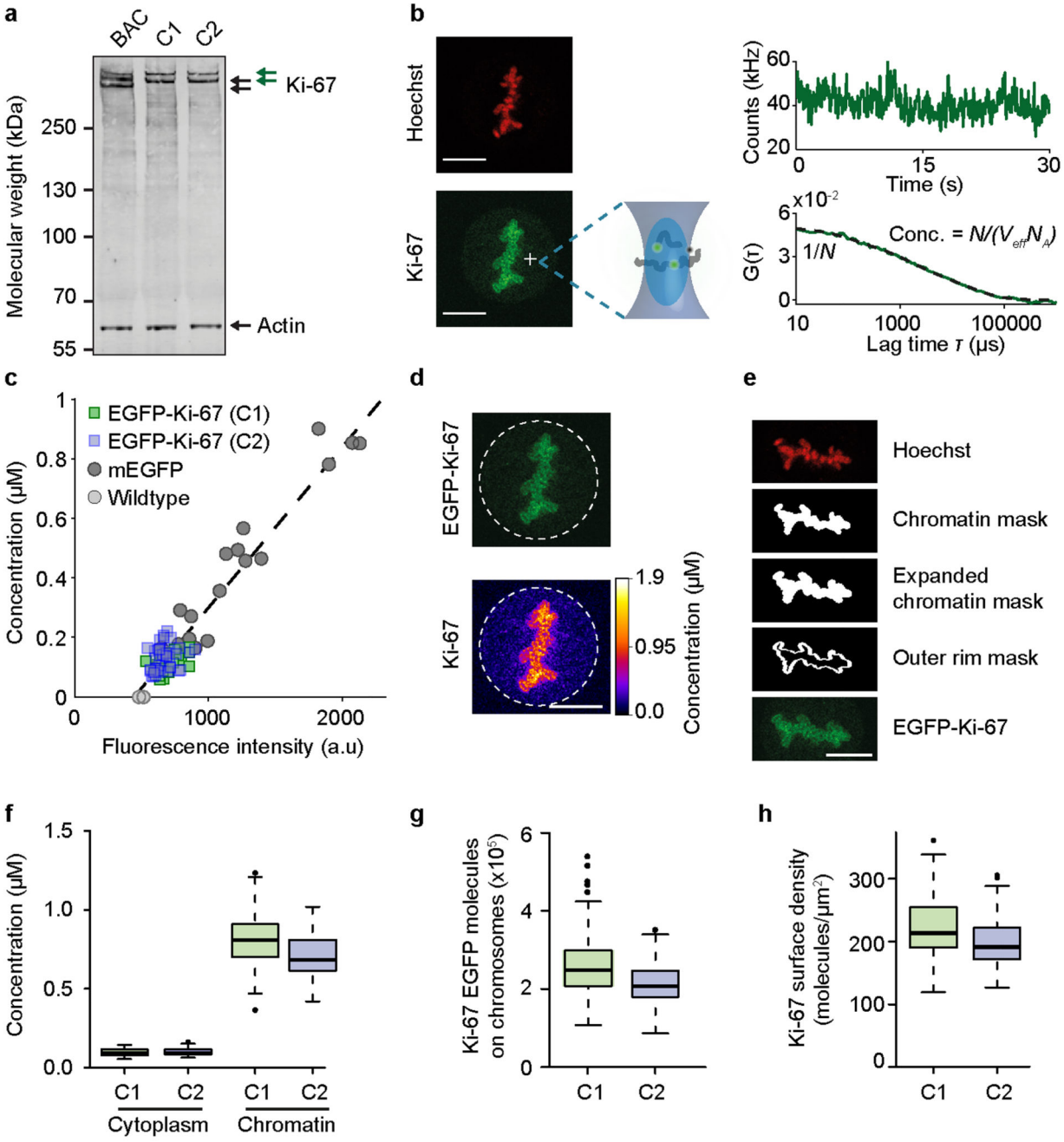

Extended Data Figure 8. Fluorescence correlation spectroscopy of endogenous Ki-67 tagged with EGFP.

a, Western blot performed on whole cell lysates of a HeLa cell line overexpressing GFP-tagged Ki-67 from a bacterial artificial chromosome (BAC), and of two different clones in which all endogenous Ki-67 alleles were N-terminally tagged with EGFP (C1, C2). The two lower bands labeled by anti Ki-67 antibody in the BAC cell line (black arrows) correspond to the two wildtype Ki-67 isoforms. The EGFP-Ki-67 versions appear upshifted (green arrows) and the band of the small EGFP-tagged isoform overlaps with the band of the wildtype large isoform. **b-h**, FCS measurement from 3 independent experiments with 111

cells (C1) and 156 cells (C2). **b**, Imaging and analysis pipeline for FCS-calibrated imaging. Metaphase cells were identified based on Hoechst staining and imaged in 3D (only the central slice is shown). In the cytoplasm of the central slice an FCS measurement was performed. From the photon counts (right upper panel) the autocorrelation function (ACF) was computed (right lower panel). From the fit of the ACF to Eq. S1 the number of particles N in the focal volume was obtained. The concentration at the FCS point was computed by dividing N by the effective focal volume Veff and the Avogadro's constant N_A. For details see Supplementary Methods. **c**, A calibration curve was obtained by plotting the concentration computed from FCS against the fluorescence intensity in a 5 x 5 pixel region at the FCS measurement point (Eq. S2, dashed line). **d**, Fluorescence microscopy image of live HeLa cell with endogenous Ki-67, labeled by EFGP, scaled to absolute Ki-67 concentration as determined by FCS. **e**, Example segmentation of chromosomes and the chromosome surface used for quantification in f-h. Segmentation was performed in 3D but for simplification only a single z-section is shown. A chromatin mask was obtained by segmentation of the Hoechst signal. To determine Ki-67 concentration on chromosomes the mask was dilated to include Ki-67 signal at the outer chromosome surface (Expanded chromatin mask). To calculate Ki-67 molecules on the outer chromosome surface, a rim around the chromatin mask was used (outer rim mask). See Supplementary Methods for details. **f-h**, Quantification of FCS measurements. Boxes indicate median, quartiles and 1.5 * interquartile range. **f**, Mean Ki-67 concentration in the cytoplasm and on 3D-segmented chromosomes using the expanded chromatin mask depicted in e. **g**, Total number of Ki-67 molecules within the whole DNA volume using the expanded chromatin mask depicted in e. **h**, Density of Ki-67 molecules on the chromosome surface using the outer rim mask depicted in e. Bars, 10 μm.

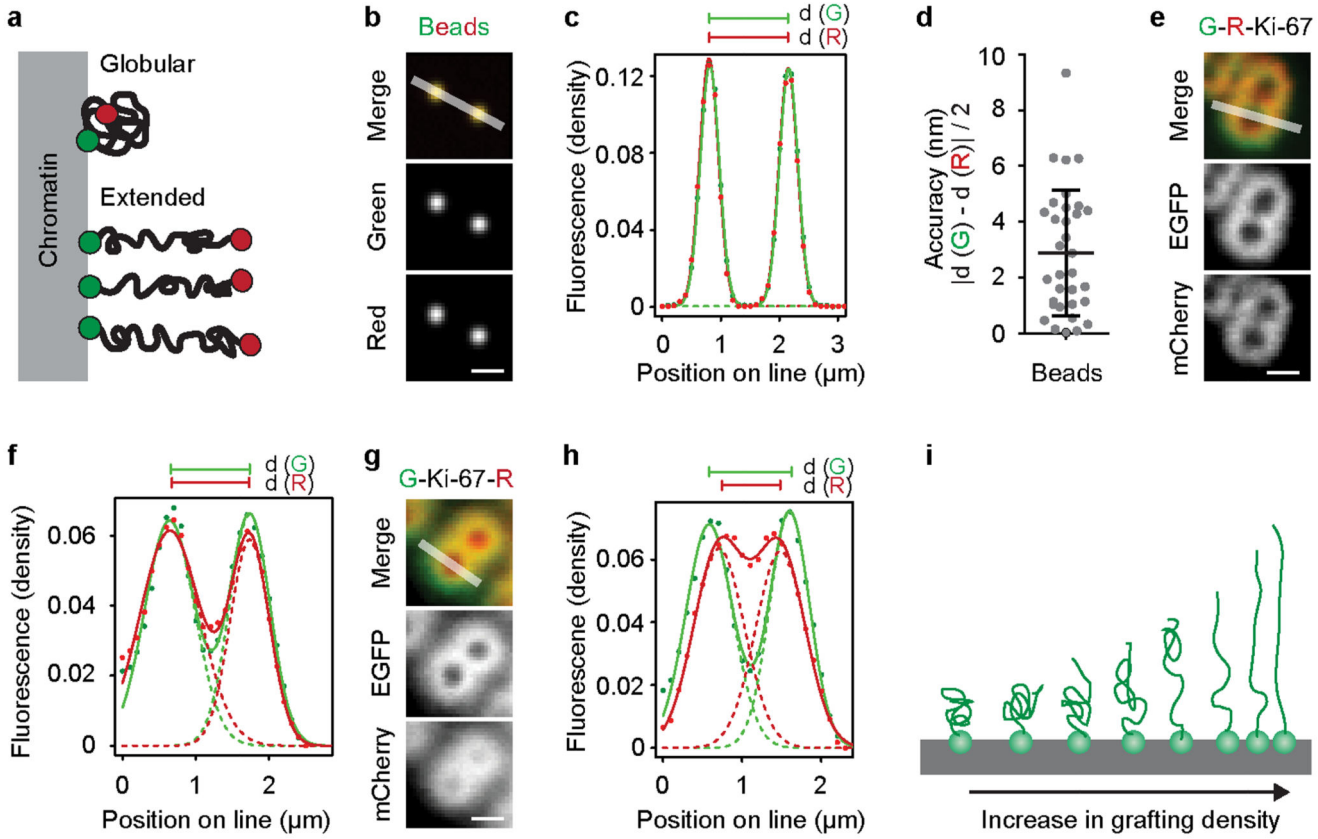

Extended Data Figure 9. Dual-color labeling of Ki-67's protein termini indicates an extended conformation oriented perpendicular to the mitotic chromosome surface.

a, Schematic of Ki-67 labeled at the N-terminus (red) and at the chromatin-binding C-terminus (green). At high densities, Ki-67 might acquire extended brush-like conformations, as known for polymeric surfactants. **b**, Multispectral fluorescent beads with 500 nm diameter were imaged as reference data to determine dual-color localization accuracy. The chromatic register shift in the green and red channel was corrected by image registration. Line profiles (white line) yielded fluorescence profiles **c**, for green and red channels. A sum of two Gaussian functions was fitted (solid line) for each channel and peak-to-peak distances of the corresponding single Gaussian functions (dotted lines) were measured for green (d(G)) and red (d(R)) channels. **d**, The accuracy of the localization method as illustrated in b, c was determined based on the absolute difference between green and red peak-to-peak distances divided by 2. Mean (black line) and standard deviation (whiskers) are indicated. **e-h**, Representative example cells of the quantification in Fig. 4c. **e**, Live HeLa wildtype cell expressing EGFP-mCherry-Ki-67. Representative example of a sister chromatid pair oriented perpendicular to the imaging plane. The line profile (white line) yielded a **f**, fluorescence profile across one sister chromatid. A sum of two Gaussian functions was fitted (solid line) for each channel and peak-to-peak distances of the corresponding single Gaussian functions (dotted lines) were measured for green (d(G)) and red (d(R)), respectively. **g**, Live HeLa wildtype cell expressing EGFP-Ki-67-mCherry. Representative example of a sister chromatid pair oriented perpendicular to the imaging plane. The line profile (white line) yielded a **h**, fluorescence profile across one sister chromatid. A sum of

Europe PMC Funders Author Manuscripts

Europe PMC Funders Author Manuscripts

two Gaussian functions was fitted (solid line) for each channel and peak-to-peak distances of the corresponding single Gaussian functions (dotted lines) were measured for green (d(G)) and red (d(R)), respectively. **i**, Model illustrating that an increased grafting density of Ki-67 at the chromosome surface might gradually increase the polymer brush height due to repulsive forces between the polymers. Bars, 1 μm.

Extended Data Table 1
Proteins ranked by predicted net charge at pH 7.

Rank in human proteome	Hugo_ID	ENSEMBL_ID	Charge
1	ASPM	ENSP00000356379	472.565
2	SRRM2	ENSP00000301740	414.8897
3	NEB	ENSP00000484342	254.7429
4	SRRM1	ENSP00000363510	170.867
5	CCDC168	ENSP00000320232	168.6658
6	ZNF729	ENSP00000469582	161.0149
7	ASH1L	ENSP00000357330	148.6947
8	HRNR	ENSP00000357791	148.3841
9	SRRM5	ENSP00000476253	143.9397
10	C2orf16	ENSP00000386190	135.8782
11	KMT2A	ENSP00000432391	134.2102
12	MUC6	ENSP00000487059	134.1865
13	**MK167**	**ENSP00000357643**	**133.9347**
14	SFI1	ENSP00000383145	130.5004
15	ZNF91	ENSP0000038272	13.3559
16	NKTR	ENSP00000232978	129.8251
17	FLG	ENSP00000357789	118.11
18	ZC3H3	ENSP00000262577	117.9798
19	ZNF99	ENSP00000380293	115.1412
20	SRRM4	ENSP00000267260	113.6421
21	RBBP6	ENSP00000317872	110.2916
22	PRPF4B	ENSP00000433547	109.6788
23	ZNF208	ENSP00000380315	107.9556
24	ZNF721	ENSP00000428878	105.6381
25	SRRM3	ENSP00000480851	104.7896
26	ZNF808	ENSP00000352846	102.4866
27	C1orf167	ENSP00000414909	101.2286
	Charge of core histones		
	HIST1H3A	ENSP00000366999	19.9270
	HIST1H2BA	ENSP00000274764	18.22513
	HIST1H4A	ENSP00000244537	17.9833
	HIST1H2AA	ENSP00000297012	15.70769

Supplementary Information

Refer to Web version on PubMed Central for supplementary material.

Acknowledgments

We thank the IMBA/IMP BioOptics microscopy facility, J. Meissner, and M.J. Hossain for technical support, H. Liu and S. Tietscher for generation of plasmids, C. Haering, M. Samwer, W. H. Gerlich, and O. Wueseke for comments on the manuscript, Life Science Editors for editing assistance, and U. Kutay for LAP2β-GFP/H2B-mRFP-expressing cells. D.G., A.A.H., J.E. have received funding from the European Community's Seventh Framework Programme FP7/2007-2013 under grant agreement n° 241548 (MitoSys), and A.Z.P, D.G. and J.E. under grant agreement n° 258068 (Systems Microscopy). D.G. has received funding from an ERC Starting Grant under agreement n° 281198 (DIVIMAGE), and from the Austrian Science Fund (FWF) project n° SFB F34-06 (Chromosome Dynamics). S.C. has received funding from a Human Frontier Science Program Long-Term Postdoctoral Fellowship and the European Community's Seventh Framework Programme FP7/2007-2013 under grant agreement n° 330114 (IEF). T.M.R. was supported by Deutsche Forschungsgemeinschaft (DFG): SPP1384 "Mechanisms of Genome Haploidization" MU 1423/3-2 and grant MU 1423/8-1.

References

1. Kschonsak M, Haering CH. Shaping mitotic chromosomes: From classical concepts to molecular mechanisms. Bioessays. 2015; 37:755–766. [PubMed: 25988527]
2. Hirano T. Condensin-Based Chromosome Organization from Bacteria to Vertebrates. Cell. 2016; 164:847–857. [PubMed: 26919425]
3. Ohta S, Wood L, Bukowski-Wills JC, Rappsilber J, Earnshaw WC. Building mitotic chromosomes. Curr Opin Cell Biol. 2011; 23:114–121. [PubMed: 20974528]
4. Naumova N, et al. Organization of the mitotic chromosome. Science. 2013; 342:948–953. [PubMed: 24200812]
5. Van Hooser AA, Yuh P, Heald R. The perichromosomal layer. Chromosoma. 2005; 114:377–388. [PubMed: 16136320]
6. Ohta S, et al. The protein composition of mitotic chromosomes determined using multiclassifier combinatorial proteomics. Cell. 2010; 142:810–821. [PubMed: 20813266]
7. Fuller BG, et al. Midzone activation of aurora B in anaphase produces an intracellular phosphorylation gradient. Nature. 2008; 453:1132–1136. [PubMed: 18463638]
8. Neumann B, et al. Phenotypic profiling of the human genome by time-lapse microscopy reveals cell division genes. Nature. 2010; 464:721–727. [PubMed: 20360735]
9. Heriche JK, et al. Integration of biological data by kernels on graph nodes allows prediction of new genes involved in mitotic chromosome condensation. Mol Biol Cell. 2014; 25:2522–2536. [PubMed: 24943848]
10. Whitfield ML, George LK, Grant GD, Perou CM. Common markers of proliferation. Nat Rev Cancer. 2006; 6:99–106. [PubMed: 16491069]
11. Yerushalmi R, Woods R, Ravdin PM, Hayes MM, Gelmon KA. Ki67 in breast cancer: prognostic and predictive potential. The Lancet Oncology. 2010; 11:174–183. [PubMed: 20152769]
12. Saiwaki T, Kotera I, Sasaki M, Takagi M, Yoneda Y. In vivo dynamics and kinetics of pKi-67: transition from a mobile to an immobile form at the onset of anaphase. Exp Cell Res. 2005; 308:123–134. [PubMed: 15896774]
13. Verheijen R, et al. Ki-67 detects a nuclear matrix-associated proliferation-related antigen. II. Localization in mitotic cells and association with chromosomes. J Cell Sci. 1989; 92(Pt 4):531–540. [PubMed: 2689459]
14. Booth DG, et al. Ki-67 is a PP1-interacting protein that organises the mitotic chromosome periphery. eLife. 2014; 3:e01641. [PubMed: 24867636]
15. Sobecki M, et al. The cell proliferation antigen Ki-67 organises heterochromatin. eLife. 2016; 5doi: 10.7554/eLife.13722
16. Vanneste D, Takagi M, Imamoto N, Vernos I. The role of Hklp2 in the stabilization and maintenance of spindle bipolarity. Curr Biol. 2009; 19:1712–1717. [PubMed: 19818619]

17. Beaudouin J, Gerlich D, Daigle N, Eils R, Ellenberg J. Nuclear envelope breakdown proceeds by microtubule-induced tearing of the lamina. Cell. 2002; 108:83–96. [PubMed: 11792323]
18. Cidado J, et al. Ki-67 is required for maintenance of cancer stem cells but not cell proliferation. Oncotarget. 2016; 7:6281–6293. [PubMed: 26823390]
19. Hofmann K, Bucher P. The FHA domain: a putative nuclear signalling domain found in protein kinases and transcription factors. Trends Biochem Sci. 1995; 20:347–349. [PubMed: 7482699]
20. Schluter C, et al. The cell proliferation-associated antigen of antibody Ki-67: a very large, ubiquitous nuclear protein with numerous repeated elements, representing a new kind of cell cycle-maintaining proteins. J Cell Biol. 1993; 123:513–522. [PubMed: 8227122]
21. Takagi M, Matsuoka Y, Kurihara T, Yoneda Y. Chmadrin: a novel Ki-67 antigen-related perichromosomal protein possibly implicated in higher order chromatin structure. J Cell Sci. 1999; 112(Pt 15):2463–2472. [PubMed: 10393802]
22. Takagi M, Sueishi M, Saiwaki T, Kametaka A, Yoneda Y. A novel nucleolar protein, NIFK, interacts with the forkhead associated domain of Ki-67 antigen in mitosis. J Biol Chem. 2001; 276:25386–25391. [PubMed: 11342549]
23. Rosen, MJ.; Kunjappu, JT. Surfactants and Interfacial Phenomena. 4th. John Wiley & Sons; 2012.
24. Milner ST. Polymer brushes. Science. 1991; 251:905–914. [PubMed: 17847384]
25. Hyman AA, Weber CA, Julicher F. Liquid-liquid phase separation in biology. Annu Rev Cell Dev Biol. 2014; 30:39–58. [PubMed: 25288112]
26. Brangwynne CP, Mitchison TJ, Hyman AA. Active liquid-like behavior of nucleoli determines their size and shape in Xenopus laevis oocytes. Proc Natl Acad Sci U S A. 2011; 108:4334–4339. [PubMed: 21368180]
27. Zwicker D, Decker M, Jaensch S, Hyman AA, Julicher F. Centrosomes are autocatalytic droplets of pericentriolar material organized by centrioles. Proc Natl Acad Sci U S A. 2014; 111:E2636–2645. [PubMed: 24979791] [**References cited in the method section only**]
28. Schmitz MH, Gerlich DW. Automated live microscopy to study mitotic gene function in fluorescent reporter cell lines. Methods Mol Biol. 2009; 545:113–134. [PubMed: 19475385]
29. Ran FA, et al. Double nicking by RNA-guided CRISPR Cas9 for enhanced genome editing specificity. Cell. 2013; 154:1380–1389. [PubMed: 23992846]
30. Guizetti J, et al. Cortical constriction during abscission involves helices of ESCRT-III-dependent filaments. Science. 2011; 331:1616–1620. [PubMed: 21310966]
31. Lukinavicius G, et al. SiR-Hoechst is a far-red DNA stain for live-cell nanoscopy. Nature communications. 2015; 6:8497.
32. Erfle H, et al. Work flow for multiplexing siRNA assays by solid-phase reverse transfection in multiwell plates. Journal of biomolecular screening. 2008; 13:575–580. [PubMed: 18599879]
33. Held M, et al. CellCognition: time-resolved phenotype annotation in high-throughput live cell imaging. Nat Methods. 2010; 7:747–754. [PubMed: 20693996]

Europe PMC Funders Author Manuscripts

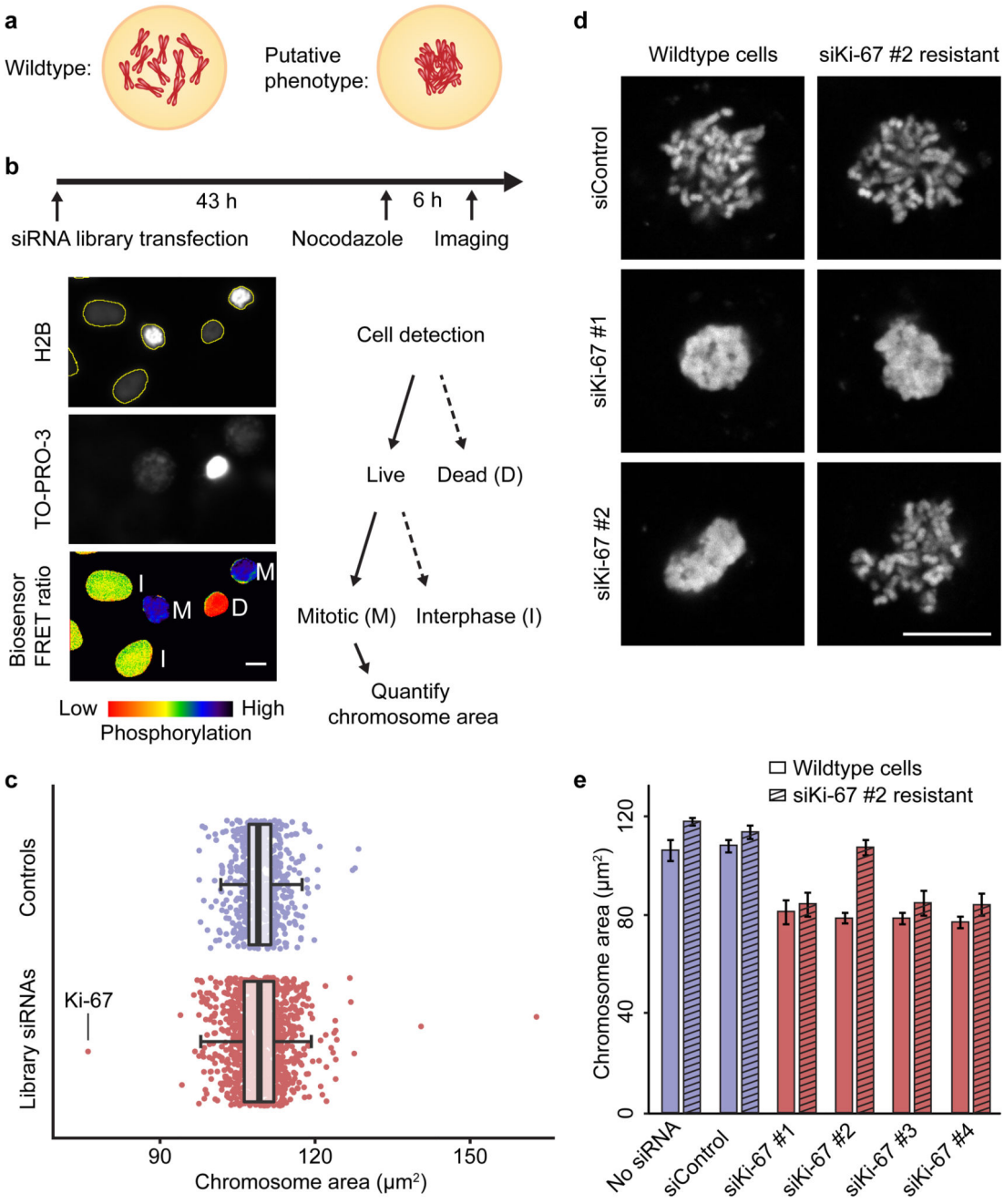

Figure 1. RNAi screen for mitotic chromosome surface adhesion regulators.

a-c, RNAi screen targeting 1295 genes. **a**, Expected chromosome phenotypes in mitotic cells with depolymerized spindles. **b**, Experimental design to detect chromosome clustering in live mitotic HeLa cells based on the viability marker TO-PRO-3 and a FRET biosensor for mitotic phosphorylation. **c**, Individual data points correspond to the median chromosome area of all live mitotic cells per target gene, based on 2 or 3 different siRNAs. Mean, quartiles, and 1.5 * interquartile range are indicated. **d-e**, Rescue of RNAi phenotype. **d**, HeLa cells, wildtype or strain mutated in siKi-67 #2 target site, were transfected as indicated

and imaged live in presence of nocodazole (n = 9-10 images per condition). **e**, Quantification of chromosome clustering as in b. The median size of the chromosome area was determined in 3 experiments (bars indicate mean ± SD, n > 71 cells per condition and experiment, for exact sample numbers see Methods). Bars, 10 μm.

Europe PMC Funders Author Manuscripts

Europe PMC Funders Author Manuscripts

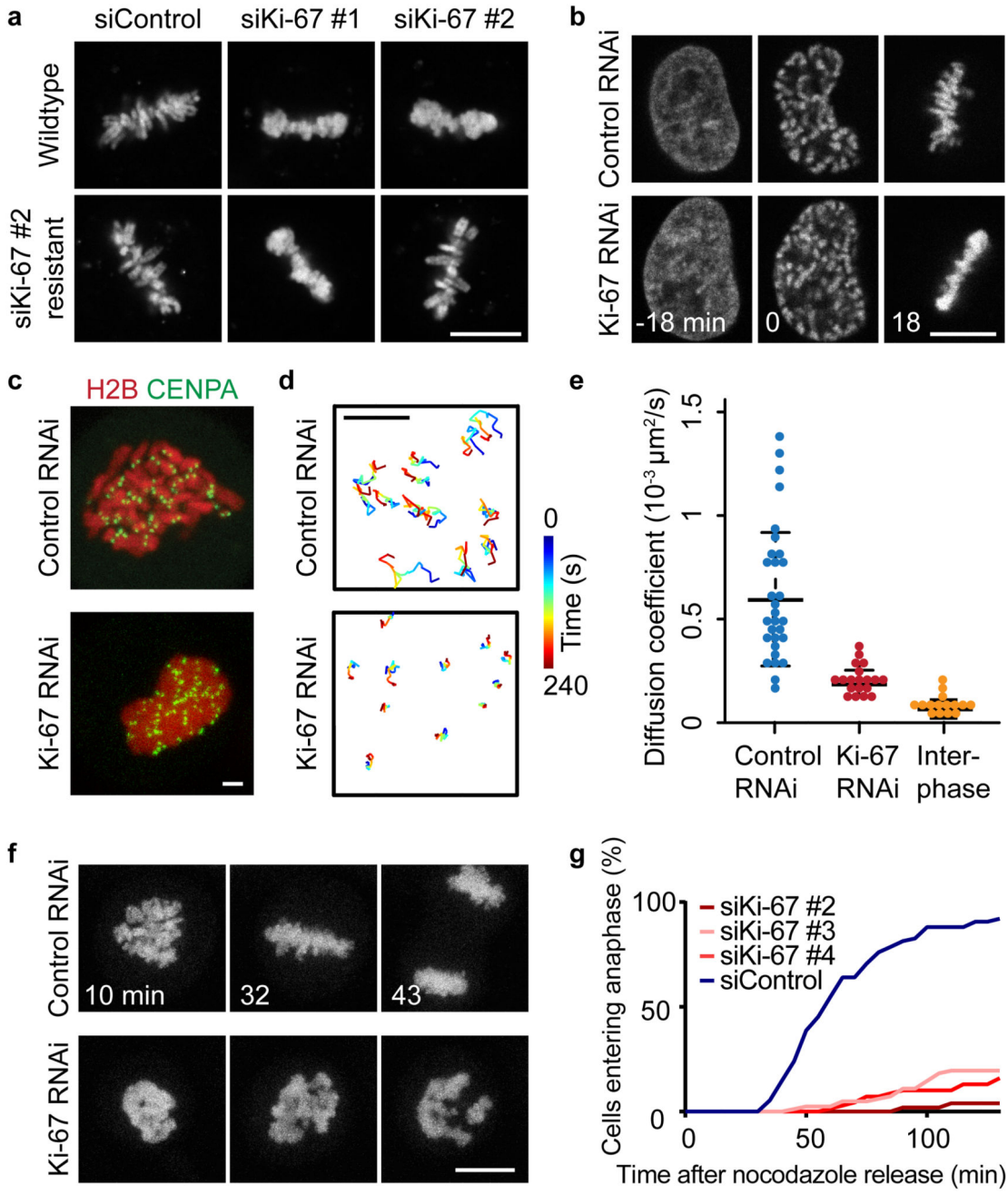

Figure 2. Spatial separation of mitotic chromosomes by Ki-67 is important for chromosome motility.

a, Live HeLa cells, wildtype or siKi-67 #2-resistant strain, transfected as indicated and stained with Hoechst. Quantified in Extended Data Fig. 2a. **b**, Time-lapse microscopy of HeLa cells expressing fluorescently-tagged H2B, transfected as indicated (NEBD, t = 0 min, n = 16 per condition). **c-e**, Kinetochore tracking. **c**, Live mitotic HeLa cells stably expressing H2B-mCherry/CENP-A-EGFP transfected with indicated siRNAs were imaged in presence of nocodazole and **d**, kinetochores were tracked in time-lapse videos. **e**, Diffusion

coefficients derived from mean square displacement (MSD) analyses. Bars indicate mean ± SD. **f**, Live mitotic HeLa cells expressing fluorescently-tagged H2B imaged after nocodazole washout (t = 0 min) **g**, were scored for anaphase entry (cumulative frequency, 3 independent experiments with total sample numbers of n = 75 (siControl), n = 51 (siKi-67 #2), n = 82 (siKi-67 #3), n = 69 (siKi-67 #4). Bars, 2 μm in c, d, all others 10 μm.

Europe PMC Funders Author Manuscripts

Europe PMC Funders Author Manuscripts

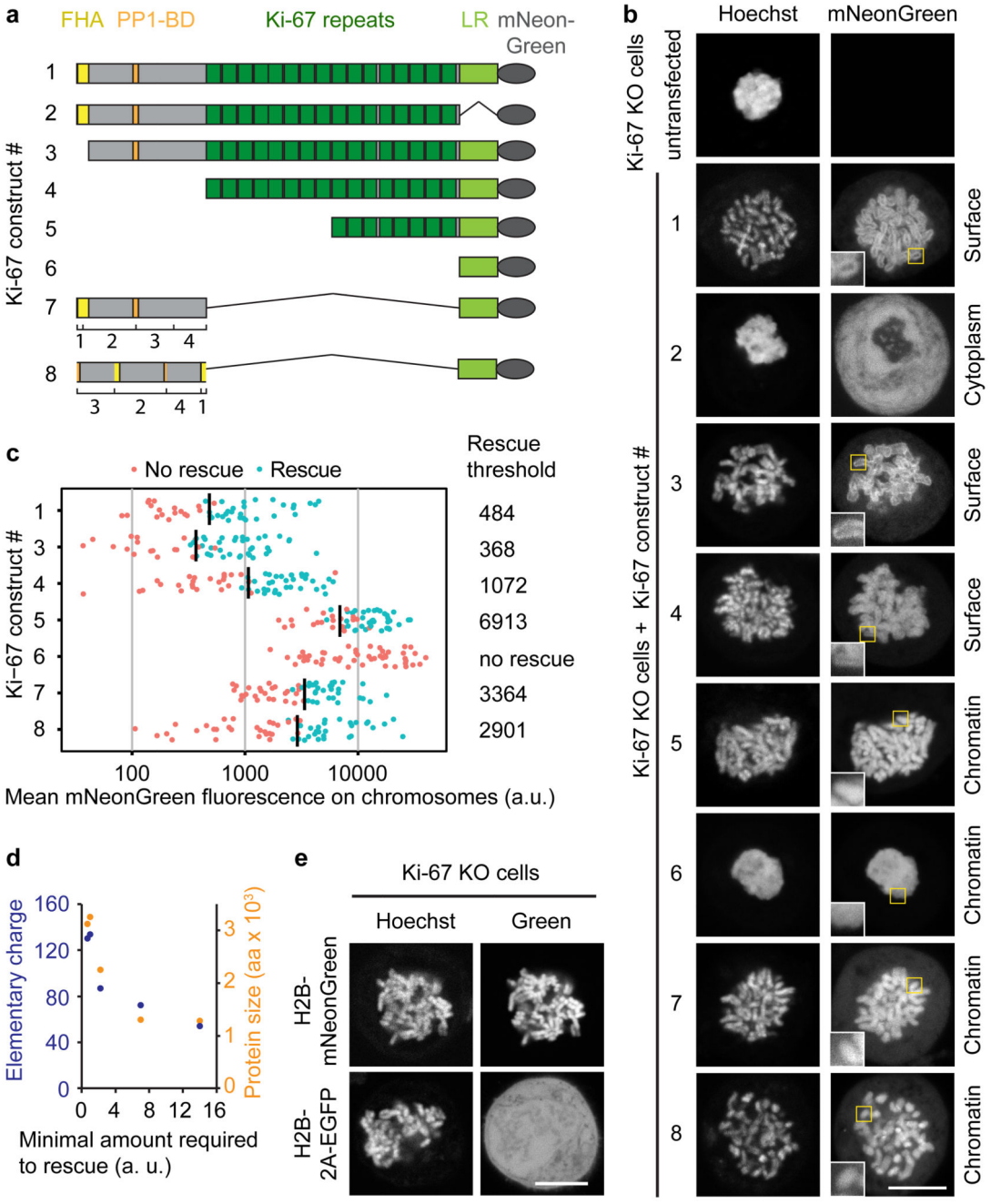

Figure 3. Ki-67's chromosome separation function is not confined within a specific subdomain.

a, Design of Ki-67 constructs. **b**, Ki-67 constructs were transfected in nocodazole-treated Ki-67 knockout HeLa cells (inserts are magnifications of yellow boxes) and **c**, analyzed for restoration of mitotic chromosome separation. Individual cells (dots) were classified by chromosome morphology (clustered: no rescue; dispersed: rescue) and plotted according to expression levels. Black bars indicate threshold required for mitotic chromosome separation. **d**, Correlation of Ki-67-truncation expression levels required for mitotic chromosome separation (as in c, relative to full length Ki-67) with their size and predicted electrical

charge at pH 7. **e**, Live Ki-67 knockout HeLa cells transfected with indicated constructs (quantified in Extended Data Fig. 7b). Bars, 10 μm.

Europe PMC Funders Author Manuscripts

Europe PMC Funders Author Manuscripts

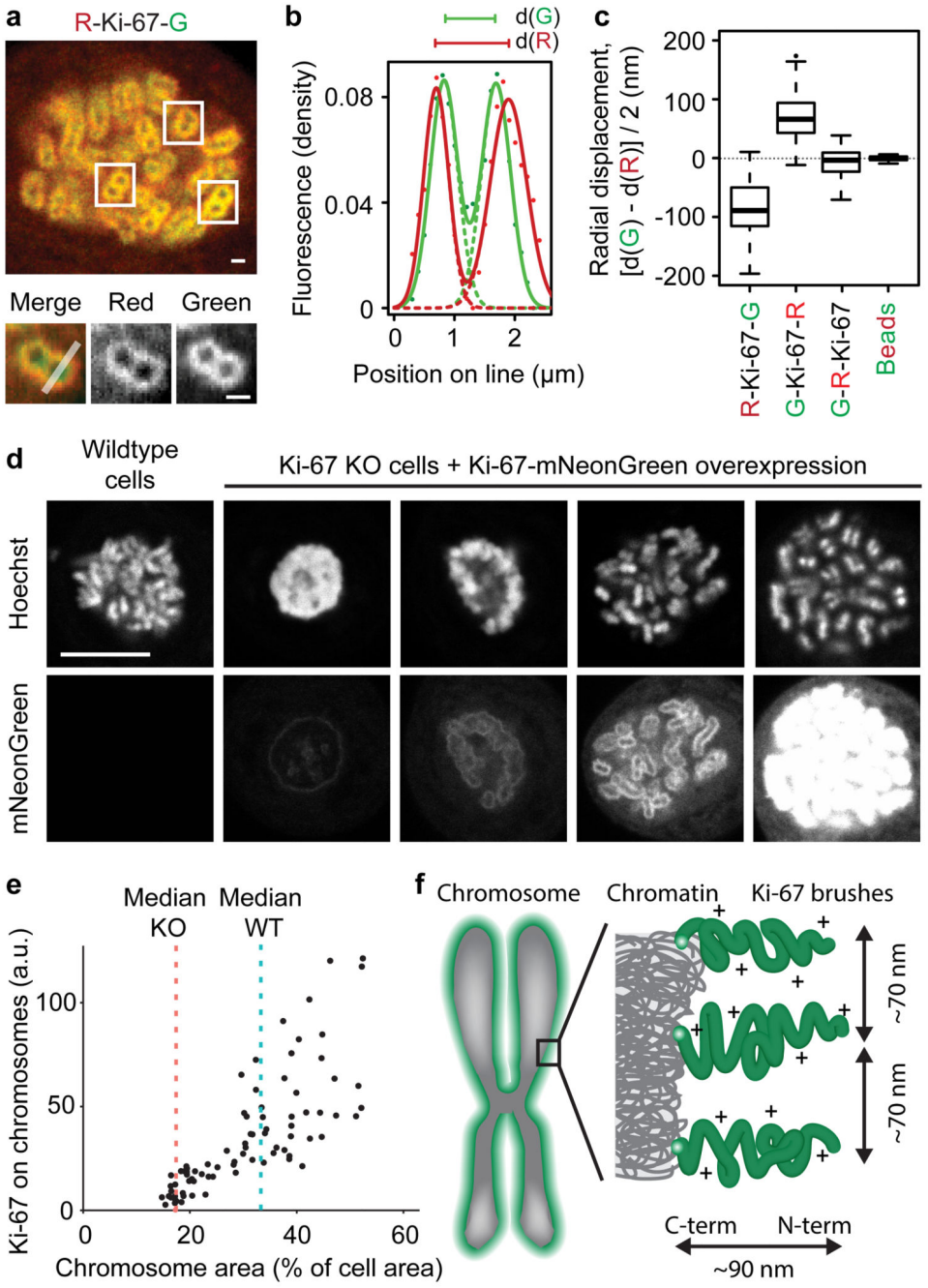

Figure 4. Densely grafted Ki-67 molecules have an extended conformation perpendicular to the chromosome surface.

a, Example of a live HeLa cell (from the analysis in c) expressing mCherry-Ki-67-EGFP. Chromosomes oriented perpendicular to the imaging plane (white boxes) were analyzed by line profiles across one sister chromatid (bottom panels; white line) and **b**, a sum of two Gaussian functions (solid line) was fitted to the line profile to measure peak-to-peak distance of the corresponding single Gaussians (dotted lines). **c**, The average distance between the labeled Ki-67 polypeptide termini along the axis perpendicular to the chromosome surface

was calculated for mCherry-Ki-67-EGFP (n = 53), EGFP-Ki-67-mCherry (n = 52), EGFP-mCherry-Ki-67 (n = 44) and multispectral fluorescent beads (n = 34). Boxes indicate median, quartiles and 1.5 * interquartile range. **d**, Live nocodazole-treated Ki-67 knockout cells expressing different levels of Ki-67-mNeonGreen **e**, were quantified with reference to chromosome area and Ki-67 levels on chromosomes (each dots represents a cell, 4 independent experiments, dashed lines indicate the median of 39 wildtype and 40 Ki-67 knockout cells). **f**, Model of Ki-67-mediated mitotic chromosome repulsion. Bars, 1 μm in a, 10 μm in d.

Europe PMC Funders Author Manuscripts